CRYSTAL GROWTH & DESIGN

Article

New Lanthanide Metalloligands and Their Use for the Assembly of Ln-Ag Bimetallic Coordination Frameworks: Stepwise Modular Synthesis, Structural Characterization, and Optical Properties

Marco Visconti, Simona Maggini, Gianfranco Ciani, Pierluigi Mercandelli, Benedetta Del Secco, Luca Prodi, Massimo Sgarzi, Nelsi Zaccheroni, and Lucia Carlucci

Cryst. Growth Des., **Just Accepted Manuscript** • DOI: 10.1021/acs.cgd.9b00894 • Publication Date (Web): 25 Jul 2019

New Lanthanide Metalloligands and Their Use for the Assembly of Ln-Ag Bimetallic Coordination Frameworks: Stepwise Modular Synthesis, Structural Characterization, and Optical Properties

Marco Visconti,[a] Simona Maggini,[a] Gianfranco Ciani,[a] Pierluigi Mercandelli,[a] Benedetta Del Secco,[b] Luca Prodi,[b] Massimo Sgarzi,[b] Nelsi Zaccheroni,[b] Lucia Carlucci,[a,*]

[a] Dipartimento di Chimica, Università degli Studi di Milano, via Golgi 19, 20133 Milano, Italy
[b] Dipartimento di Chimica "Giacomo Ciamician", Università degli Studi di Bologna, via Selmi 2, 40126 Bologna, Italy

Abstract

Stepwise self-assembly processes using new lanthanide metalloligands (Ln-MLs) and silver salts have been successfully applied to isolate 4f-4d heterometallic coordination networks of four different structural types. In particular, the new lanthanide tetrakis-chelate complexes $NEt_4[Ln(L^1)_4]$ [HL^1 = 1,3-bis(4′-cyanophenyl)-1,3-propanedione; Ln = Eu (**1a**), La (**1b**), Nd (**1c**), Tb (**1d**)] and $NEt_4[Ln(L^2)_4]$ (HL^2 = 1,3-bis(4′-pyridyl)-1,3-propanedione; Ln = Eu (**1e**), Nd (**1f**)] have been synthetized, characterized and reacted with different silver salts. The use of $NEt_4[Ln(L^1)_4]$ allowed then to isolate and characterize *i*) neutral one-dimensional ladder-like species of formula $[Ln(L^1)_4Ag]$ [Ln = Eu (**2a**), La(**2b**), Nd(**2c**), Tb(**2d**)] and *ii*) their supramolecular isomers $[Ln(L^1)_4Ag]$ [Ln = Eu (**3a**), La (**3b**), Nd (**3c**), Tb (**3d**)] showing a very unstable 2D network structure, *iii*) the cationic 2D species $[Ln(L^1)_4Ag_2]X$ [Ln = Eu, X = PF_6^-, $CF_3SO_3^-$, ClO_4^- (**4a**–**4c**); Ln = Tb, Nd, La X = PF_6^- (**4d**–**4f**)] and, only for lanthanum, *iv*) a fourth 2D species of formula $[La(L^1)_4(H_2O)Ag]$ (**5**) and **sql** topology. Of the eight nitrile groups on the MLs potentially coordinating, only a partial number is used for networking with Ag(I), that is, only two in families **2** and **3**, and four in family **4** and in network **5**. Finally, the four structural types are rationalized in terms of a new "pincer-like" Secondary Building Unit (SBU) consisting of a silver cation coordinating two central carbon atoms (γ carbon) of two different diketonate ligands on the same ML. Therefore, it is shown that compounds **5**, **4** and **2**–**3** contain, respectively, none, one or two of such pincer-like SBUs. The luminescence properties of the Ln-MLs and some of their polymeric species have been also investigated in solution and in the solid state.

1 Introduction

Metal-organic frameworks (MOFs), a class of crystalline porous materials built up by linking together metal cations or clusters and organic ligands, have attracted great and increasing attention from the scientific community in the last decades mainly for their inherent incredible versatility. Their structures, in fact, can be easily engineered by using the SBU approach and the principles of reticular chemistry to get specific network topologies and tailored properties.[1–4]

Their application has been proposed in a wide variety of fields including, among others, ion exchange,[5] catalysis,[6] sensing,[7] magnetism,[8] light emitting and display devices,[9,10] gas adsorption and reversible storage,[11,12] taking often advantage from the possibility to develop multifunctional MOFs.[13]

In this exciting and very lively context heterometallic f-d metal-organic frameworks (HMOFs), containing lanthanide ions together with transition metal ions as nodes, represent a very important family thanks to the peculiar and unique photophysical properties of f-block-based materials.[14,15] Their very distinguishable and narrow emission, ranging from UV to NIR, grants the possibility to obtain high quantum yield and brightness (depending from the metal cation environment) and also to use them in technologically relevant devices. Moreover, these lanthanide ions usually show

coordination numbers ranging from 6 to 12 allowing for the preparation of more versatile building blocks in comparison with the transition metal ions, even if less predictable during the design step.
In recent times great interest in the crystal engineering of HMOFs has been especially focused on the step-by-step synthetic strategy based on the use of metalloligands.[16–19] Preformed and sometimes also independently characterized metalloligand complexes (MLs), as self-existing entities, have been employed with different metal ions for the assembly of frameworks exhibiting interesting and useful topologies; by this way a better control of the building up process is expected. However, while many cases have been reported of f-d arrays (both extended or finite molecular entities), constructed either using transition metal metalloligands[20–22] or following some kind of one-pot synthetic route with mixed hard/soft Lewis base ligands,[23–25] a very limited number of Ln-metalloligands used in the preparation of HMOFs have been described until now.
One of the first examples was reported by Shimizu et al.[26–28] who synthetized the luminescent complex [Ln(4,4′-disulfo-2,2′-bipyridine *N*,*N*′-dioxide)$_3$(H_2O)$_2$] (Ln = Sm, Eu, Gd, Tb, Dy) and reacted it in situ with Ba(II) to obtain an isostructural series of microporous luminescent HMOFs. More recently, the stepwise strategy based on the lanthanide ML [Ln(3-TPyMNTB)$_2$]ClO_4 [Ln = Eu, Gd; 3-TPyMNTB = tris((pyridin-3-ylmethyl)benzimidazol-2-ylmethyl)amine] has been successfully used to assemble Eu-Ag and Gd-Ag HMOFs. Particularly interesting is the europium derivative that shows white light emitting properties.[29] The same strategy has been also successfully used to assemble Ln-Cd HMOFs, not easily accessible by other way, utilizing the complex [Ln(ODA)$_3$]$_3$ (H_2ODA = oxydiacetic acid) as ML.[30–33] A mixed Gd-Co HMOF has been recently synthetized by a stepwise reaction between the Ln-ML [Gd(H_2CAM)$_3$]·5¼H_2O (H_2CAM = chelidamic acid) and cobalt nitrate.[34]
Combination of lanthanide metalloligands and transition metal ions in one metal-organic framework could represent a suitable way for isolating new convenient materials with interesting luminescent properties for different applications. We previously employed the metalloligand approach to assemble heterometallic MOFs of different transition metals by developing new M(II) and M(III) tris-chelate complexes of 1,3-functionalized β-diketone ligands (HL^1 = 1,3-bis(4′-cyanophenyl)-1,3-propanedione and HL^2 = 1,3-bis(4′-pyridyl)-1,3-propanedione). In particular, HL^1 based MLs when reacted with AgX salts afforded a rich family of porous 3D heterometallic networks with the same 6-fold interpenetrated **pcu** topology and interesting reversible anion-exchange properties.[35] On the other hand, by the same approach the ML [Fe(L^2)$_3$] allowed to isolate 2D and 3D polymeric networks with structures depending on the nature of the counter-anions.[36]
Here we examined the possibility to obtain new Ln-metalloligands using the previously described[35,36] functionalised β-diketone ligands HL^1 and HL^2 (Scheme 1) as the first step for the synthesis of novel f-d HMOFs. We had the parallel aims to explore a new and convenient synthetic approach and to investigate the influence of different environments on the possible emissive properties of these materials.

Scheme 1. Structure of the two ligands HL^1 and HL^2

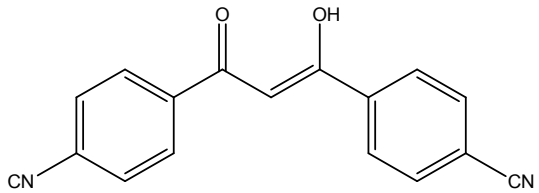

HL^1

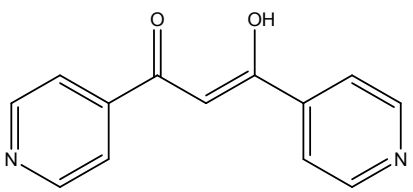

HL^2

We report here the preparation and structural characterization of two tetrakis-chelate metalloligands [Ln(L^1)$_4$]$^-$ (Ln = Eu, La, Nd, Tb) and [Ln(L^2)$_4$]$^-$ (Ln = Eu, Nd**)**, that were successively reacted with a variety of metal salts (Scheme 2). At present, crystalline products were obtained and investigated only by using the [Ln(L^1)$_4$]$^-$ metalloligands with silver salts of different anions (X^-). Four different types of heterometallic polymeric frameworks were isolated, depending on the counter-anion and/or

the reaction conditions. These include *i*) a series of 1D polymers with formula $[Ln(L^1)_4Ag]$, *ii*) a family of unstable 2D networks with the same composition $[Ln(L^1)_4Ag]$, *i.e.* supramolecular isomers, *iii*) a family of 2D cationic frames $[Ln(L^1)_4Ag_2]X$ with different Ln and/or X^- counterion and *iv*) the 2D polymer $[La(L^1)_4(H_2O)Ag]$. The characterized structures show the variable donor ability of the metalloligands that, interestingly, can provide for networking with silver ions not only the nitrile donor groups but also the central carbon atoms (γ carbon) of their diketonate ligands.

2 Experimental section

2.1 General procedures

All employed commercial reagents and solvents (Sigma-Aldrich) were of high-grade purity and used as supplied, without further purification. The ligands HL^1 and HL^2 were prepared according to published procedures.[35,36] All manipulations were performed under aerobic conditions unless standard Schlenk techniques were required. Anhydrous tetrahydrofuran was freshly distilled under nitrogen from sodium/benzophenone. NMR spectra were recorded on Bruker AC300 or AC400 instruments; δ values are given in ppm relative to tetramethylsilane. Infrared spectra were collected on a PerkinElmer PARAGON 1000 FT-IR spectrometer. Thermogravimetric analysis (TGA) were performed on a PerkinElmer TGA 7 instrument under dynamic nitrogen (total flow rate 20 cm^3/min) with a ramp rate of 10°C/min in the range 30–650°C. X-ray powder diffraction (PXRD) patterns were recorded on a Philips PW1820 diffractometer (Cu Kα radiation, λ = 1.5418 Å), in the 5–35° 2θ range (0.02° and 2.5 s per step). Elemental analyses were carried out at the Microanalytical Laboratory of the University of Milan with a PerkinElmer 2400 instrument.

2.2 Photophysical Measurements

Photochemical experiments were carried out at room temperature in solutions and in solid phase and at 77 K in liquid nitrogen. Solid phase spectra were recorded on samples prepared inserting the solid powders or crystals between two square thin microscope glasses sealed with some double-sided tape while a common quartz cuvette (1 cm optical path) for samples in solution. A UV/VIS spectrophotometer PerkinElmer Lambda 650 was used to measure absorption spectra. Emission spectra were recorded with an Edinburgh FLS920 equipped photomultiplier Hamamatsu R928P and the same instrument connected to a PCS900 PC card was used for the Time Correlated Single Photon Counting (TCSPC) experiments to measure fluorescence lifetimes. Phosphorescence lifetimes were recorded with a PerkinElmer LS-55. Luminescence quantum yields (uncertainty, ±20%) were obtained by SPHEREOPTICS general purpose integration sphere 4″, spectraflect coating 1 baffle 0+/90*, following the De Mello method to record and process data.
Fluorescence intensities were corrected, when required, for inner filter effects according to standard methods.[37]

2.3 Synthesis of $NEt_4[Ln(L^1)_4]$ [Ln = Eu (1a, 1a*), La (1b), Nd (1c), Tb (1d)]

Complexes **1a–1d** were synthetized with similar procedures on using the corresponding lanthanide salts. Only the synthesis of **1a** is here reported in detail. The ligand HL^1 (500.0 mg, 1.82 mmol) was suspended under stirring in 50 mL of ethanol and treated with NEt_4OH (35% aqueous solution, 908.5 mg, 2.159 mmol). After slow addition of $Eu(NO_3)_3 \cdot 5H_2O$ (196.4 mg, 0.459 mmol) dissolved in 15 mL of ethanol, a yellow solid starts immediately to precipitate. The reaction mixture was left to stir at room temperature for 16 h. Compound **1a** was recovered as a yellow solid after filtration, washing with ethanol, and drying in air. Yield: 82.6%. Elemental Analysis (%): Calcd for $C_{76}H_{56}EuN_9O_8$: C 66.37, H 4.10, N 9.17; Found: C 64.31, H 4.01, N 9.42. IR (KBr, cm^{-1}) ν: 3068 (w), 2985 (w), 2226 (s), 1596 (vs), 1546 (s), 1520 (vs), 1488 (vs), 1457 (vs), 1393 (s), 1306 (s), 1294 (s), 1276 (sh), 1218 (m), 1173 (w), 1105 (m), 1056 (m), 1016 (m), 839 (w), 859 (s), 779 (s), 695 (m), 671 (w), 643 (w),

580 (m), 547 (m), 470 (m). ^{1}H NMR (300 MHz, d_6-acetone) δ: 8.00 (d, 16 H), 7.70 (d, 16H), 6.21 (s, 4 H), 3.54 (q, 8H), 1.43 (t, 12 H).

1b: Yield 82.0%. Elemental Analysis (%): Calcd for $C_{76}H_{56}LaN_9O_8$: C 67.01, H 4.14, N 9.25; Found: C 66.29, H 4.25, N 9.26. IR (KBr, cm^{-1}) ν: 3062 (w), 3042 (w), 2988 (w), 2227 (s), 1595 (vs), 1546 (vs), 1518 (vs), 1487 (vs), 1456 (vs), 1393 (vs), 1305 (s), 1292 (s), 1272 (sh), 1217 (s), 1174 (m), 1105 (m), 1053 (m), 1016 (s), 1000 (m), 938 (w), 857 (s), 817 (s), 779 (s), 752 (sh), 694 (m), 670 (m), 642 (w), 578 (m), 546 (s), 467 (m). ^{1}H NMR (300 MHz, d_6-acetone) δ: 8.23 (d, 16 H), 7.76 (d, 16H), 6.82 (s, 4 H), 3.51 (q, 8 H), 1.41 (t, 12 H).

1c: Yield 70.6%. Elemental Analysis (%): Calcd for $C_{76}H_{56}N_9NdO_8$: C 66.75, H 4.13, N 9.22; Found: C 64.56, H 4.26, N 9.52. IR (KBr, cm^{-1}) 3065(w), 3042(w), 2990(w), 2227(s), 1595(vs), 1547(vs), 1519(vs), 1487(vs), 1457(vs), 1398(vs), 1308(s), 1293(s), 1217(s), 1174(m), 1111(m), 1055(m), 1016(s), 1005(m), 940(w), 852(s), 819(s), 779(s), 694(m), 670(m), 643(w), 578(m), 542(s), 463(m). ^{1}H NMR (300 MHz, d_6-acetone) δ: 8.64 (broad, 16 H), 8.14 (broad, 16H), 9.44 (broad, 4 H), 3.47 (q, 8 H), 1.36 (t, 12 H).

1d: Yield 73.6%. Elemental Analysis (%): Calcd for $C_{76}H_{56}N_9O_8Tb$: C 66.04, H 4.08, N 9.12; Found: C 68.19, H 3.96, N 8.98. IR (KBr, cm^{-1}) 3066(w), 3044(w), 2988(w), 2227(s), 1594(vs), 1545(vs), 1518(vs), 1487(vs), 1456(vs), 1395(vs), 1305(s), 1298(s), 1278(sh), 1215(s), 1174(m), 1101(m), 1054(m), 1016(s), 1013(m), 936(w), 857(s), 817(s), 785(s), 698(m), 674(m), 642(w), 578(m), 546(s), 467(m).

Single crystals of **1a** and **1a*** were obtained by slow diffusion into dichloromethane solutions of **1a** of liquid or vapors of hexane, respectively. PXRD patterns of the bulk solids are comparable to those of the corresponding grinded single crystals. They differ from the patterns calculated on the bases of the single-crystal structures possibly as a consequence of structural changes induced by the loss of chlatrated solvents (Figures S1 and S2).

2.4 Synthesis of $NEt_4[Ln(L^2)_4]$ [Ln = Eu (1e), Nd (1f)]

Compounds **1e** and **1f** were obtained by the same procedure on using the proper lanthanide nitrate salt. Only the synthesis of **1e** is here reported in detail. The ligand HL^2 (201.2 mg, 0.889 mmol) was suspended in 5.5 mL of ethanol and treated with NEt_4OH (35% aqueous solution, 423.3 mg, 1.006 mmol). 3 mL of an ethanol solution of $Eu(NO_3)_3 \cdot 5H_2O$ (94.2 mg, 0.220 mmol) were slowly added to the mixture which was left under stirring for 3 h. The addition of 14 mL of ethyl acetate causes the precipitation of compound **1e** as a yellow solid which was recovered by filtration, washed with water, and dried in air. Yield: 62.9%. Elemental Analysis (%): Calcd for $C_{60}H_{56}EuN_9O_8$: C 60.91, H 4.77, N 10.65; Found: C 62.13, H 4.71, N 11.11. IR (KBr, cm^{-1}) ν: 3060 (s), 3032 (s), 2984 (s), 2952 (s), 2892 (m), 1654 (sh, s), 1602 (vs), 1560 (s), 1540 (vs), 1522 (vs), 1458 (vs), 1430 (vs), 1384 (vs), 1320 (s), 1284 (s), 1218 (s), 1184 (s), 1172 (s), 1134 (m), 1082 (m), 1060 (s), 998 (s), 944 (s), 880 (w), 850, 772 (s), 720 (s), 690 (s), 664 (m), 610 (s), 522 (m), 458 (w), 432 (w). ^{1}H NMR (300 MHz, d_6-acetone) δ: 8.47 (d, 16H), 7.67 (d, 16H) 6.05 (s, 4H) 3.55 (q, 8H) 1.44 (t, 12H).

1f: Yield 59.7%. Elemental Analysis (%): Calcd for $C_{60}H_{56}N_9NdO_8$: C 61.31, H 4.80, N 10.72; Found: C 64.16, H 4.99, N 11.23. IR (KBr, cm^{-1}) ν: 3056 (s), 3034 (s), 2983 (s), 2951 (s), 2892 (m), 1654 (sh, s), 1602 (vs), 1560 (s), 1540 (vs), 1522 (vs), 1458 (vs), 1430 (vs), 1384 (vs), 1320 (s), 1281 (s), 1217 (s), 1184 (s), 1174 (s), 1145 (m), 1083 (m), 1061 (s), 700 (s), 944 (s), 883 (w), 856, 773 (s), 721 (s), 667 (s), 664 (m), 612 (s), 523 (m). ^{1}H NMR (300 MHz, d_6-acetone) δ: 8.64 (d, 16H), 8.15 (d, 16H) 7.70 (s, 4H) 3.47 (q, 8H) 1.35 (t, 12H).

Single crystals of **1e** and **1f** suitable for X-ray diffraction analyses were grown by slow diffusion of ethyl ether into a dichloromethane solution of the corresponding compound.

2.5 Synthesis of 1D $[Ln(L^1)_4Ag]$ [Ln = Eu (2a), La (2b), Nd (2c), Tb (2d)]

Microcrystalline samples of **2a**–**2d** were obtained by the same procedure using compounds **1a**–**1c** as starting reagents. Only the synthesis of **2a** is here reported in detail. Silver tosylate (10.6 mg, 0.0380 mmol) was dissolved in 6 mL of ethanol/water (5:1 v/v) mixture and added drop by drop over 15

minutes to an acetonitrile solution (5 mL) of **1a** (50.8 mg, 0.0369 mmol). The mixture was left under stirring at room temperature for 15 h. A yellow solid formed which was collected on a Büchner funnel, washed with ethanol, and dried in air to give compound **2a**. Yield 60.3%. Elemental Analysis (%): Calcd for $C_{68}H_{36}AgEuN_8O_8$: C 60.37, H 2.68, N 8.28; Found: C 59.83, H 2.64, N 8.42. IR (KBr, cm^{-1}) ν: 3088 (w) 3070 (w), 2981 (w), 2228 (s), 1595 (vs), 1547 (vs), 1519 (vs), 1488 (vs), 1447 (vs), 1394 (s), 1306 (s), 1295 (s), 1276 (sh), 1218 (s), 1178 (w), 1105 (m), 1056 (m), 1018 (m), 938 (w), 857 (s), 781 (s), 697 (m), 670 (w), 643 (w), 584 (m), 547 (m), 471 (m). Thermogravimetric analysis of **2a** is reported in Figure S3.

2b Yield 73%. Elemental Analysis (%): Calcd for $C_{68}H_{36}AgLaN_8O_8$: C 60.96, H 2.71, N 8.36; Found: C 58.97, H 2.61, N 8.20. IR (KBr, cm^{-1}) ν: 3068 (w), 3048 (sh), 2228 (s), 1594 (vs), 1545 (vs), 1518 (vs), 1487 (vs), 1442 (vs), 1392 (vs), 1306 (s), 1293 (s), 1272 (sh), 1218 (s), 1178 (w), 1106 (m), 1054 (m), 1017 (s), 936 (w), 857 (s), 780 (s), 696 (m), 673 (w), 643 (w), 582 (m), 547 (s), 469 (m).

2c Yield 40.6%. Elemental Analysis (%): Calcd for $C_{68}H_{36}AgN_8NdO_8$: C 60.72, H 2.70, N 8.33; Found: C 62.11, H 2.78, N 8.04. IR (KBr, cm^{-1}) ν: 3075 (w), 3050 (sh), 2227 (s), 1594 (vs), 1545 (vs), 1518 (vs), 1488 (vs), 1442 (vs), 1391 (vs), 1306 (s), 1293 (s), 1218 (s), 1174 (w), 1088 (m), 1054 (m), 1015 (s), 936 (w), 853 (s), 780 (s), 696 (m), 666 (w), 643 (w), 583 (m), 547 (s), 473 (m).

2d Yield 41.5%. Elemental Analysis (%): Calcd for $C_{68}H_{36}AgN_8O_8Tb$: C 60.06, H 2.67, N 8.24; Found: C 57.46, H 2.58, N 8.05. IR (KBr, cm^{-1}) ν: 3073 (w), 3044 (sh), 2228 (s), 1595 (vs), 1545 (vs), 1517 (vs), 1490 (vs), 1444 (vs), 1393 (vs), 1306 (s), 1295 (s), 1272 (sh), 1218 (s), 1173 (w), 1116 (m), 1054 (m), 1017 (s), 936 (w), 856 (s), 782 (s), 695 (m), 670 (w), 643 (w), 585 (m), 547 (s), 470 (m).

Single crystals of **2a**–**2d** suitable for X-ray analysis were obtained by slow diffusion of an acetonitrile/water (5:1 v/v) solution of silver tosylate in an acetonitrile solution of the proper MLs (**1a**–**1d**) in 3 days. PXRD patterns of the bulk solids are comparable to the patterns calculated on the bases of the corresponding single-crystal structures, taking into account the limited crystallinity of the samples (Figure S4).

2.6 Synthesis of 2D [Ln(L^1)$_4$Ag] [Ln = Eu (3a), La (3b), Nd (3c), Tb (3d)]

Microcrystalline samples of polymers **3a**–**3d** were obtained by the same procedure using compounds **1a**–**1d** as starting reagents. Only the synthesis of **3b** is here reported in detail. A solution of silver tosylate (20.5 mg, 0.074 mmol) in water (10 mL) was added drop by drop in a period of 1 h to a solution of **1b** (100.2 mg, 0.074 mmol) dissolved in acetonitrile (10 mL). The mixture was left under stirring for 3 h. A yellow solid formed which was collected by filtration on a Büchner funnel, washed with ethanol, and dried in air to give compound **3b**. Yield 79.3%. Elemental Analysis (%): Calcd for $C_{68}H_{36}LaN_8O_8$: C 60.96, H 2.71, N 8.36; Found: C 60.97, H 2.58, N 8.44. IR (KBr, cm^{-1}) ν: 3097 (w), 3073 (w), 2933 (vw), 2227 (s), 1596 (vs), 1547 (vs), 1519 (vs), 1488 (vs), 1451 (vs), 1434 (sh, vs), 1393 (s), 1305 (m), 1295 (s), 1277 (sh, m), 1216 (m), 1178 (w), 1107 (m), 1055 (m), 1017 (M), 943 (w), 857 (m), 782 (s), 700 (m), 671 (w), 645 (w), 583 (w), 547 (m), 469 (m).

3a Yield 78.2%. Elemental Analysis (%): Calcd for $C_{68}H_{36}AgEuN_8O_8$: C 60.37, H 2.68, N 8.28; Found: C 59.35, H 2.64, N 8.56. IR (KBr, cm^{-1}) ν: 3090 (w), 3071 (w), 2929 (vw), 2228 (s), 1596 (vs), 1547 (vs), 1519 (vs), 1488 (vs), 1451 (vs), 1432 (sh, vs), 1393 (s), 1307 (m), 1295 (s), 1277 (sh, m), 1217 (m), 1178 (w), 1109 (m), 1056 (m), 1017 (m), 938 (w), 857 (m), 783 (s), 697 (m), 671 (w), 643 (w), 583 (w), 547 (m), 471 (m).

3c Yield 84%. Elemental Analysis (%): Calcd for $C_{68}H_{36}AgN_8NdO_8$: C 60.72, H 2.70, N 8.33; Found: C 63.61, H 2.60, N 8.29. IR (KBr, cm^{-1}) ν: 3082 (w), 3073 (w), 2922 (vw), 2226 (s), 1596 (vs), 1547 (vs), 1519 (vs), 1488 (vs), 1451 (vs), 1432 (sh, vs), 1393 (s), 1306 (m), 1295 (s), 1276 (sh, m), 1215 (m), 1178 (w), 1107 (m), 1056 (m), 1017 (m), 939 (w), 857 (m), 785 (s), 697 (m), 671 (w), 646 (w), 584 (w), 546 (m), 470 (m).

3d Yield 90.1%. Elemental Analysis (%): Calcd for $C_{68}H_{36}AgN_8O_8Tb$: C 60.06, H 2.67, N 8.24; Found: C 60.00, H 2.55, N 8.07. IR (KBr, cm^{-1}) ν: 3088 (w), 3077 (w), 2943 (vw), 2228 (s), 1595

(vs), 1546 (vs), 1520 (vs), 1488 (vs), 1451 (vs), 1433 (sh, vs), 1397 (s), 1309 (m), 1297 (s), 1216 (m), 1178 (w), 1107 (m), 1056 (m), 1017 (m), 940 (w), 857 (m), 781 (s), 697 (m), 671 (w), 647 (w), 585 (w), 545 (m), 471 (m).

Yellow needle-shaped crystals of **3b** used for X-ray analysis were obtained by slow diffusion of an acetonitrile solution of **1b** into a water solution of $[Ag(CH_3CN)_4]BF_4$ in 3 days.

Despite the good agreement between the patterns collected for the powders of **3a**–**3c**, the comparison with the pattern calculated from the partial data collected for the single crystal of **3b** is very lacking (Figure S5). This result can be safely attributed to the highly unstable nature of the structure of **3**, that did not allow a complete single-crystal structural characterization even at low temperature.

2.7 Synthesis of 2D $[Ln(L^1)_4Ag_2]X$ [Ln = Eu, X = PF_6, ClO_4, CF_3SO_3 (4a–4c); Ln = La, Nd, Tb, X = PF_6 (4d–4f)]

Microcrystalline samples of polymers **4a**–**4f** were obtained by the same procedure using compounds **1b**–**1c** as starting reagents and the proper silver salts. Only the synthesis of **4a** is here reported in detail. A solution of silver hexafluorophosphate (19.2 mg, 0.076 mmol) in ethanol (8 mL) was added drop by drop in a period of 15 minutes to a solution of **1a** (51.2 mg, 0.037 mmol) dissolved in dichloromethane (8 mL). The mixture was left under stirring for 3 h. A yellow solid formed which was collected by filtration on a Büchner funnel, washed with ethanol, and dried in air to obtain compound **4a**. Yield 93%. Elemental Analysis (%): Calcd for $C_{68}H_{36}N_8O_8Ag_2EuF_6P$: C 50.86, H 2.26, N 6.98; Found: C 52.00, H 2.32, N 6.95. IR (KBr, cm^{-1}) ν: 3096 (w), 3071 (w), 2976 (w), 2247 (sh, m), 2230 (m), 1595 (vs), 1546 (vs), 1520 (vs), 1488 (vs), 1449 (vs), 1394 (s), 1309 (m), 1296 (s), 1276 (sh, s), 1223 (m), 1179 (w), 1106 (m), 1056 (w), 1016 (m), 938 (w), 837 (sh, s), 851 (s), 781 (s), 698 (m), 670 (w), 644 (w), 586 (w), 558 (m), 548 (m), 472 (w).

4b Yield 95%. Elemental Analysis (%): Calcd for $C_{68}H_{36}Ag_2ClEuN_8O_{12}$: C 52.35, H 2.32, N 7.18; Found: C 50.56, H 2.33, N 7.13. IR (KBr, cm^{-1}) ν: 3095 (w), 3070 (w), 2974 (w), 2230 (s), 1595 (s), 1546 (vs), 1521 (vs), 1487 (s), 1449 (s), 1394 (s), 1308 (s), 1296 (s), 1277 (sh), 1223 (s), 1168 (m), 1015 [s, ν(Cl–O), ClO_4^-], 1057 (m), 1017 (m), 938 (w), 859 (m), 780 (s), 698 (m), 645 (m), 583 (w), 547 (m), 472 (m).

4c Yield 91%. Elemental Analysis (%): Calcd for $C_{69}H_{36}Ag_2EuF_3N_8O_{11}S$: C 51.48, H 2.25, N 8.24; Found: C 49.52, H 2.21, N 8.30. IR (KBr, cm^{-1}) ν: 3093 (w), 3069 (w), 2974 (w), 2230 (s), 1595 (vs), 1546 (vs), 1521 (vs), 1489 (vs), 1451 (vs), 1394 (s), 1308 (s), 1295 (s), 1278 (sh), 1260 (sh, ν(C–F), $CF_3SO_3^-$), 1225 (s), 1168 (m), 1106 (m), 1057 (m), 1017 (m), 938 (w), 859 (m), 780 (s), 698 (m), 671 (w, δ(C-F), $CF_3SO_3^-$), 641 (m), 583 (w), 548 (m), 472 (m).

4d Yield 92%. Elemental Analysis (%): Calcd for $C_{68}H_{36}N_8O_8Ag_2F_6LaP$: C 51.28, H 2.28, N 7.04; Found: C 52.15, H 2.38, N 6.88. IR (KBr, cm^{-1}) ν: 3096 (w), 3070 (w), 2973 (w), 2247 (sh), 2230 (s), 1595 (vs), 1545 (vs), 1519 (vs), 1488 (vs), 1445 (vs), 1392 (vs), 1308 (s), 1295 (s), 1276 (sh), 1222 (s), 1179 (w), 1106 (m), 1054 (m), 1016 (m), 936 (w), 850 (s), 838 (sh), 780 (s), 698 (m), 644 (w), 583 (w), 558 (m), 548 (m), 470 (m).

4e Yield 93%. Elemental Analysis (%): Calcd for $C_{68}H_{36}Ag_2F_6N_8NdO_8P$: C 51.11, H 2.27, N 7.01; Found: C 53.14, H 2.24, N 6.67. IR (KBr, cm^{-1}) ν: 3096 (w), 3073 (w), 2974 (w), 2247 (sh, m), 2230 (m), 1595 (vs), 1545 (vs), 1520 (vs), 1488 (vs), 1449 (vs), 1395 (s), 1310 (m), 1296 (s), 1276 (sh, s), 1223 (m), 1179 (w), 1106 (m), 1056 (w), 1016 (m), 938 (w), 837 (sh, s), 851 (s), 781 (s), 698 (m), 670 (w), 644 (w), 586 (w), 558 (m), 548 (m), 472 (w).

4f Yield 95%. Elemental Analysis (%): Calcd for $C_{68}H_{36}Ag_2F_6N_8O_8PTb$: C 50.64, H 2.25 N 6.95; Found: C 50.62, H 2.25, N 7.21. IR (KBr, cm^{-1}) ν: 3095 (w), 3072 (w), 2974 (w), 2247 (sh, m), 2230 (m), 1595 (vs), 1546 (vs), 1520 (vs), 1488 (vs), 1450 (vs), 13964 (s), 1309 (m), 1296 (s), 1276 (sh, s), 1223 (m), 1179 (w), 1106 (m), 1056 (w), 1016 (m), 938 (w), 837 (sh, s), 851 (s), 781 (s), 698 (m), 670 (w), 644 (w), 586 (w), 558 (w), 552 (w), 472 (w).

Thermogravimetric analyses of **4a**–**4d** are reported in Figure S6. Yellow plate-shaped crystals of **4a** and **4b** suitable for X-ray analysis were obtained by slow diffusion of an ethanol solution of $AgPF_6$

or $AgClO_4$ into a CH_2Cl_2 solution of **1a** in 5 days. PXRD patterns of the bulk solids are comparable to the patterns calculated on the bases of the corresponding single-crystal structures, taking into account the limited crystallinity of the samples (Figures S7 and S8).

2.8 Synthesis of 2D [La(L^1)$_4$(H$_2$O)Ag] (5)

A solution of silver tosylate (20.8 mg, 0.075 mmol) in water (10 mL) was added drop by drop in about 30 seconds to a solution of **1b** (101.0 mg, 0.074 mmol) dissolved in acetonitrile (10 mL). The mixture was left under stirring for 3 h. A yellow solid formed which was collected by filtration on a Büchner funnel, washed with water and acetonitrile, and dried in air. Yield: 95.2%. Elemental Analysis (%): Calcd for $C_{68}H_{38}AgLaN_8O_9$: C 60,15, H 2.82, N 8.25; Found: C 61.23, H 2.71, N 8.10. IR (KBr, cm^{-1}) ν: 3093 (w), 3077 (w), 2924 (w), 2250 (s), 2228 (s), 1598 (vs), 1546 (vs), 1514 (vs), 1489 (vs), 1428 (vs), 1389 (s), 1306 (s), 1293 (s), 1270 (s), 1222 (s), 1175 (m), 1108 (s), 1052 (m), 1014 (s), 936 (w), 861 (sh, s), 856 (s), 788 (s), 777 (sh, s), 758 (m), 692 (s), 678 (m), 643 (w), 578 (m), 551 (m), 546 (m), 535 (m), 475 (s).
Thermogravimetric analysis of **5** is reported in Figure S9. Yellow needle-shaped crystals of **5** suitable for X-ray analysis were obtained by slow diffusion of an acetonitrile solution of $[Ag(CH_3CN)_4]BF_4$ into a water solution of **1b** in 1 month. PXRD pattern of the bulk solid is comparable to the pattern calculated on the bases of the corresponding single-crystal structure (Figure S10).

2.9 Crystallography

Crystal data for the metalloligands **1a**, **1a***, **1e**, and **1f** and for the heterometallic MOFs **2a**, **2c**, **2d**, **4a**, and **5** are listed in Table S1 (Supporting Information). Data were collected on a Bruker APEXII-CCD diffractometer using Mo Ka radiation (λ = 0.71073 Å). Empirical absorption corrections (SADABS)[38] were applied to all data. The structures were solved by direct methods (SIR97)[39] and refined by full-matrix leasts quares on F^2 (SHELX-2014)[40] using the WINGX interface.[41] All hydrogen atoms were placed in geometrically calculated positions and subsequently refined using a riding model with $U_{iso}(H) = 1.2\ U_{eq}(C)$. Anisotropic thermal parameters were assigned to all non-hydrogen atoms, except for the clathrate solvent molecules (**1a** and **1f**: dichloromethane; **1a***: 3 dichloromethane; **1e**: water; **2a** and **2c**: ½ acetonitrile; **2d**: ½ acetone) that have been modelled also for the disorder. Further details on the refinements of the observed disordered groups can be found in the cif files. Crystals of **3b** proved to be highly unstable and a full refinement was not possible. A model was found and the coordinates are reported in the supplementary materials. All crystals were kept under mineral oil and the data collections were done at 150 K to limit decomposition. For **4a** it was difficult to refine a consistent model for the solvent molecules so their contribution was subtracted from the observed structure factors according to the BYPASS procedure[42] as implemented in PLATON[43] with the command SQUEEZE, and the PF_6^- anion was modelled isotropically over two equally occupied position.
Crystal data and selected bond distances and angles for all the characterized species are reported in Tables S1–S6. The diagrams were produced using ToposPro[44] and Mercury[45] programs. CCDC 1910771–1910779 contain the supplementary crystallographic data for this paper. These data can be obtained free of charge from The Cambridge Crystallographic Data Centre.

3 Results and discussion

3.1 Syntheses and crystal structures of the lanthanide metalloligands

3.1.1 $NEt_4[Ln(L^1)_4]$ [Ln = Eu (1a, 1a*), La (1b), Nd (1c), Tb (1d)]

Complexes **1a**–**1d** were synthetized in good yields by reacting HL^1, tetraethylammonium hydroxide and the corresponding lanthanide nitrate salts (4:4:1 ratio) in ethanol under stirring overnight at room temperature. The compounds were isolated as yellow microcrystalline solids and were characterized by XRD, IR, and ^1H NMR analyses. Crystallization by slow diffusion of liquid or vapors of hexane into dichloromethane solutions of **1a** produced single crystals whose X-ray diffraction analyses revealed to belong to different crystalline forms, namely $NEt_4[Eu(L^1)_4]\cdot CH_2Cl_2$ (**1a**) and $NEt_4[Eu(L^1)_4]\cdot 3CH_2Cl_2$ (**1a***). Both structures crystallize in the *P*–1 space group and differ in the number of clathrate dichlomethane molecules. Crystals of **1a** and **1a*** easily desolvate in the air at room temperature to give microcrystalline materials. Monitoring of such desolvation processes by X-ray powder diffraction show changes in the powder patterns up to the complete removal of clathrate molecules and convergence to similar powder patterns, thus indicating the transformation to the same crystalline phase for desolvated **1a** and **1a*** (Figure S1). Microcrystalline powders of compounds **1b**–**1d** are similar to desolvated powders of **1a** and **1a***, as evidenced by comparison of their respective PXRD patterns (Figure S2).

The asymmetric units of both **1a** and **1a*** contain one tetrakis-chelate anionic complex, one tetraethylammonium cation and, respectively, one and three dichloromethane molecules. A view of the tetrakis-chelate complex in the crystal structure of **1a** is reported in Figure 1. Views with labeling schemes for **1a** and **1a*** are shown in Figure S11. Europium centers in both compounds coordinate eight oxygen atoms belonging to four crystallographic different β-diketonate ligands (L^1) adopting coordination geometries intermediate between triangular dodecahedron (*DD*-8) and square antiprism (*SAPR*-8), the two ideal geometries for coordination number eight.

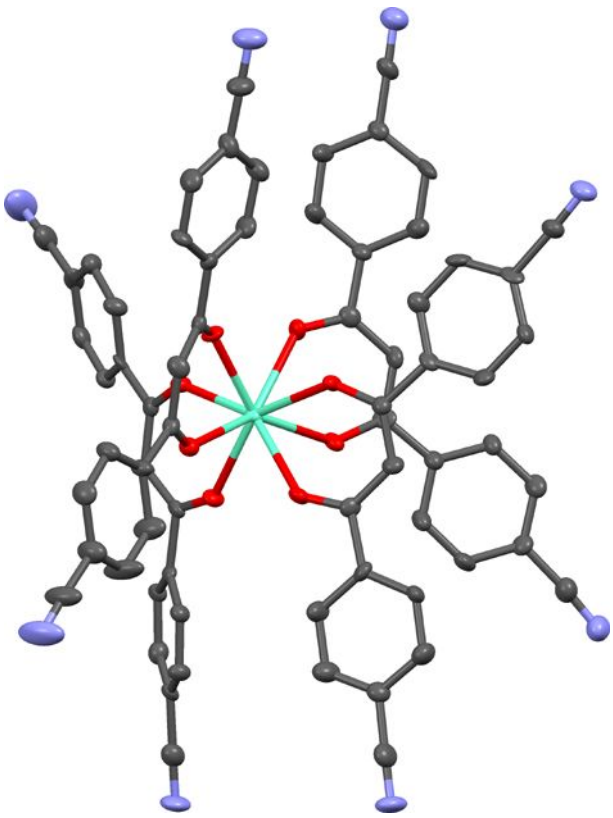

Figure 1. View of the europium complex in **1a**. Hydrogen atoms have been omitted for clarity. Ellipsoids are drawn at 50% of probability.

Average values for the Eu–O distances (2.38 and 2.39 Å in **1a** and **1a***, respectively) and for the O–Eu–O bite angles of the diketonate ligands (69.5 and 70.1 in **1a** and **1a***, respectively) are very similar in the two pseudopolymorphs. Such Eu–O distance and bite angle values are fully comparable to those of similar tetrakis-chelate β-diketonate europium complexes. In both compounds the six-membered chelate rings are folded along the O···O vector with dihedral angles between the EuO_2 plane and the plane of the ligand (defined by the two oxygen atoms and the γ-carbon atom) in the range 4.0(4)–28.6(4)° for **1a** and 16.73(13)–25.46(14)° for **1a***. Such values are comparable to those observed in other tetrakis-chelate lanthanide diketonate complexes and differences can be safely attributed to packing effects.

More generally, differences in the europium coordination geometries between **1a** and **1a*** are not significant and easily ascribable to differences in crystal packing, induced by the different number of clathrate dichloromethane molecules. No particular intermolecular interactions are present in the two crystal structures except for a face to face π-π interaction between phenyl rings belonging to the same ligand of two different adjacent complexes, which are related by an inversion center, found only in **1a***(angle between mean planes of phenyl rings 3.13(17)°, centroid to centroid distance 3.605(2) Å). Europium complexes, in both structures, are arranged along rows, with the tetraethyl ammonium and the solvent molecules disposed in the inter-row regions (Figure S12).

3.1.2 $NEt_4[Ln(L^2)_4]$ [Ln = Eu (1e), Nd (1f)]

Compounds **1e** and **1f** were obtained as yellow microcrystalline powders by reacting at room temperature europium or neodymium nitrate with four-fold equivalents of HL^2 in ethanol/water mixtures in the presence of excess amounts of tetraethylammonium hydroxide. The two compounds were characterized by XRD, IR, and ^1H NMR analyses. Single crystals of **1e** and **1f** suitable for X-ray diffraction analyses were grown by slow diffusion of ethyl ether into a dichloromethane solution of the corresponding compound. They crystallize in the space group $P2_1/c$ as solvates $NEt_4[Eu(L^2)_4]\cdot H_2O$ (**1e**) and $NEt_4[Nd(L^2)_4]\cdot CH_2Cl_2$ (**1f**). Views of the two lanthanide complexes with labelling schemes are shown in Figure S12.

The asymmetric unit of **1e** contains the europium complex, a tetraethylammonium cation and a water molecule. Europium atom is coordinated to eight oxygen atoms of four crystallographically independent chelating ligands adopting a coordination geometry intermediate between *DD*-8 and *SAPR*-8. The Eu–O distances average value is 2.38 Å and the average bite angle O–Eu–O of the chelate diketonate ligands is 70.2°, comparable with the values found for **1a** and **1a***. The six-chelate rings are folded along the O···O vector, showing dihedral angles in the range 18.60(14)–27.55(14)°.

The asymmetric unit of **1f** contains two neodymium complexes, two tetraethylammonium cations and two dichloromethane molecules. Also in this structure all the chelating ligands are crystallographically independent. The two neodymium complexes in the asymmetric unit do not show significant differences and their geometrical parameters are very similar (Table S4). In particular, the average values for the Nd–O distances are 2.43 and 2.44 Å, while the average bite angles O–Nd–O of the chelate diketonate ligands are 69.0 and 69.2°, respectively. Again the six-chelate rings are folded along the O···O vector showing dihedral angles in the range 25.60(12)– 31.51(13)° and 21.83(12)–33.18(12)°, respectively.

The europium and neodymium anionic complexes in the two crystal structures pack along rows, while the tetraethylammonium cations and the clathrate solvent molecules (water and dichloromethane) are located between these rows. In **1e** the water molecule is hydrogen bonded to a pyridyl nitrogen atom (O1w···N8, 2.94 Å).

Lanthanide complexes of pyridyl substituted β-diketonate are uncommon. The complex $[Eu(HL^2)_3(H_2L^2)]Cl_4\cdot EtOH$ [46] is the only known example of a tetrakis-chelate containing four bispyridyl-β-diketonate ligands, even if in this species three ligands are monoprotonated zwitterions and one is a doubly protonated cation. All other reported examples contain solvent molecules coordinated to the lanthanide metals and less than four chelating ligands.[47–51]

3.2 Lanthanides-silver coordination networks assembled with the $[Ln(L^1)_4]^-$ metalloligands

The reactivity of the $NEt_4[Ln(L^1)_4]$ metalloligands was investigated with different metal salts. In spite of the many attempts, single crystals suitable for X-ray diffraction analysis were isolated only using silver salts of various anions. We have isolated by this way four different families of polymeric Ln-Ag species, with distinct topology, in which the starting metalloligand moieties are essentially preserved. We have also identified the factors that can possibly drive the formation of the different products.

Metalloligands $[Ln(L^1)_4]^-$ possess eight donor nitrile groups that can be potentially employed for networking; however, in the HMOFs prepared only 2 or 4 groups out of the 8 are coordinated to silver. Moreover, as often observed in β-diketonate complexes,[52–55] the central carbon atom (methine or γ-carbon) can also form bonds towards external metal ions. We have previously described tris-chelated metalloligands with the same β-diketonate ligands that give networks with silver cations exhibiting Ag–C bonds, with bond distances in the range 2.451(11)–2.531(7) Å.[35]

The high flexibility in the stereochemistry of these metalloligands allows for the formation of a new type of Secondary Building Unit (SBU) in the reaction with silver cations. This SBU consists of a "pincer-like" moiety, in which a silver cation coordinates to two central carbon atoms of two different diketonate ligands of the same metalloligand (Figure 2). The different polymeric products could be organized on the basis of the number of these SBUs. Accordingly, species with 0, 1, and 2 "silver-pincers" *per* ML have been obtained.

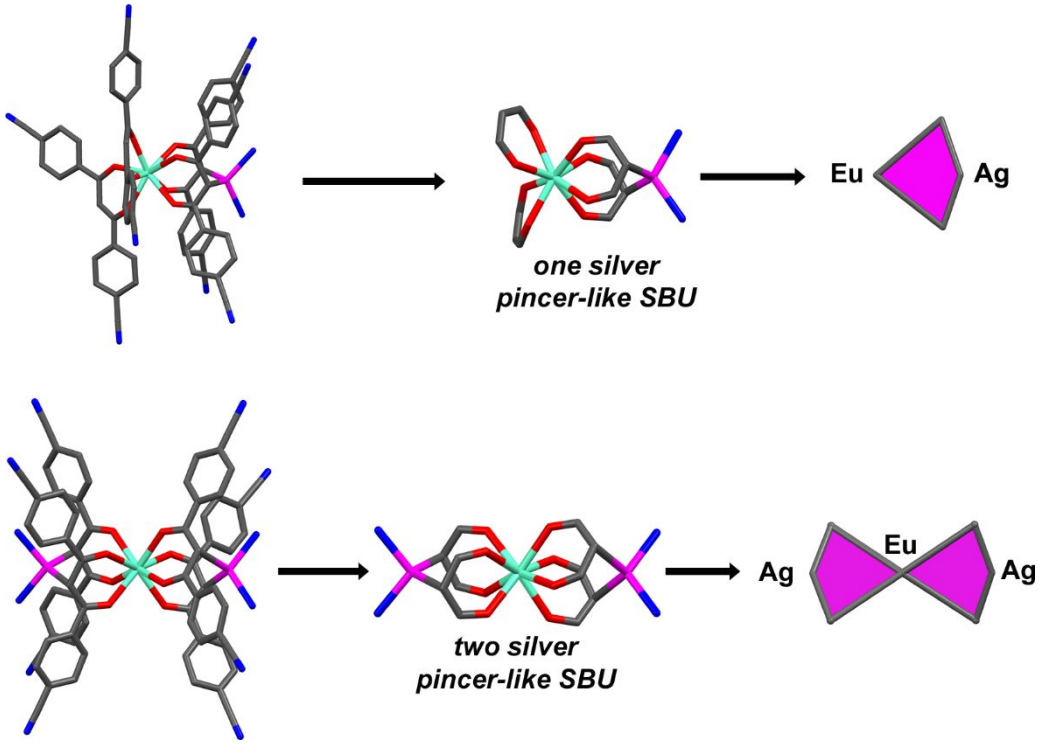

Figure 2. Schematic representation of the silver pincer-like SBUs observed in two polymer families described below. One silver-pincer like SBU (top) is formed by one ML and one silver cation interacting with the central carbon atoms of two diketonate ligands. Such neutral SBU is present in polymeric families **2** and **3**. Two silver pincer-like SBUs (bottom) are formed by one ML and two silver cations, each of which interacts with the central carbon atoms of two diketonate ligands. Such cationic SBU is present in polymeric family **4**.

Moreover, a relevant distinction to be underlined is related to the dimension of the lanthanide ion. Using MLs of Tb, Eu, and Nd only three different polymers have been obtained, while with the ML of the bigger La cation an additional fourth polymeric species can be obtained (see below). Scheme 2 collects the synthetic experimental conditions used to obtain all of the polymeric products based on the nitrile functionalized Ln-MLs $NEt_4[Ln(L^1)_4]$.

Scheme 2. Experimental conditions for the synthesis of the 1D and 2D polymeric families 2–5

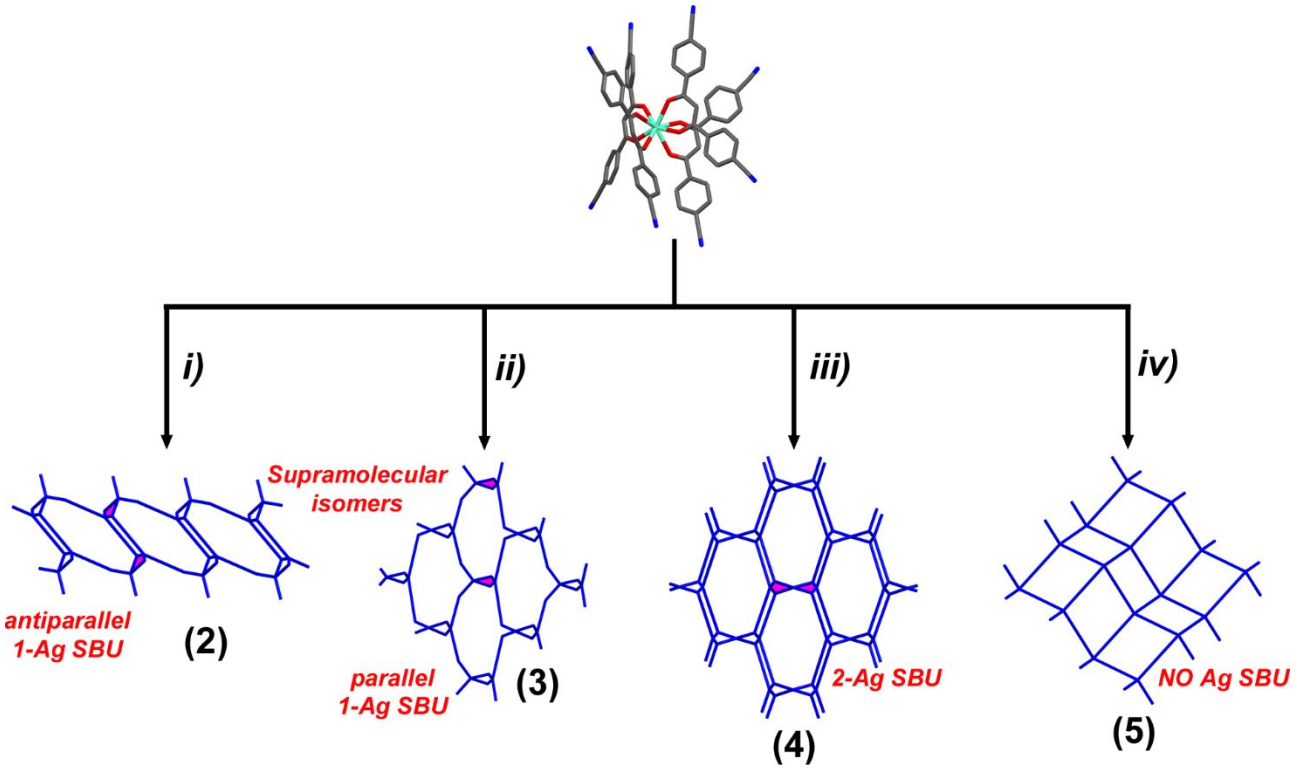

i) $CH_3C_6H_4SO_3Ag$/**1a**–**1d**, stoichiometric ratio 1:1, EtOH/H_2O (5:1)/CH_3CN; ii) $CH_3C_6H_4SO_3Ag$/**1a**–**1d**, stoichiometric ratio 1:1, H_2O/CH_3CN, slow mixing; iii) AgX/**1a**–**1d**, stoichiometric ratio 2:1, X = PF_6^-, ClO_4^-, $CF_3SO_3^-$, EtOH/CH_2Cl_2; iv) $CH_3C_6H_4SO_3Ag$/**1b**, stoichiometric ratio 1:1, H_2O/CH_3CN, fast mixing. During the crystallization of **3b** and **4b**, solvent mediated slow transformations to **5** have been evidenced.

The key factors for the synthesis of these compounds are the Ag:ML ratio and the solvent system used in the different preparations. We will now proceed to analyze in detail the different polymeric products.

3.2.1 1D coordination networks [Ln(L^1)$_4$Ag] (2a–2d)

The reactions of all ~~the~~ metalloligands with various silver salts (tosylate, triflate, hexafluorophosphate, and tetrafluoroborate) in a stoichiometric ratio of 1:1 and in different solvent systems (mixtures of ethanol, acetonitrile, water, and acetone) generate the species [Ln(L^1)$_4$Ag] [Ln = Eu, La, Nd, and Tb (**2a**–**2d**)]. Though the polymers can be prepared in many different conditions, best results are obtained when the reaction is performed using silver tosylate in ethanol/water (5:1)/acetonitrile as solvent system. In the synthesis of this family of coordination networks, only the stoichiometric ratio ML/Ag of 1:1 and the presence of small amount of water seems to be crucial.
All the crystals of the family are isomorphous and belong to the triclinic system, space group *P*–1. Their structures contain the same ladder-like 1D network depicted in Figure 3 for **2a**.

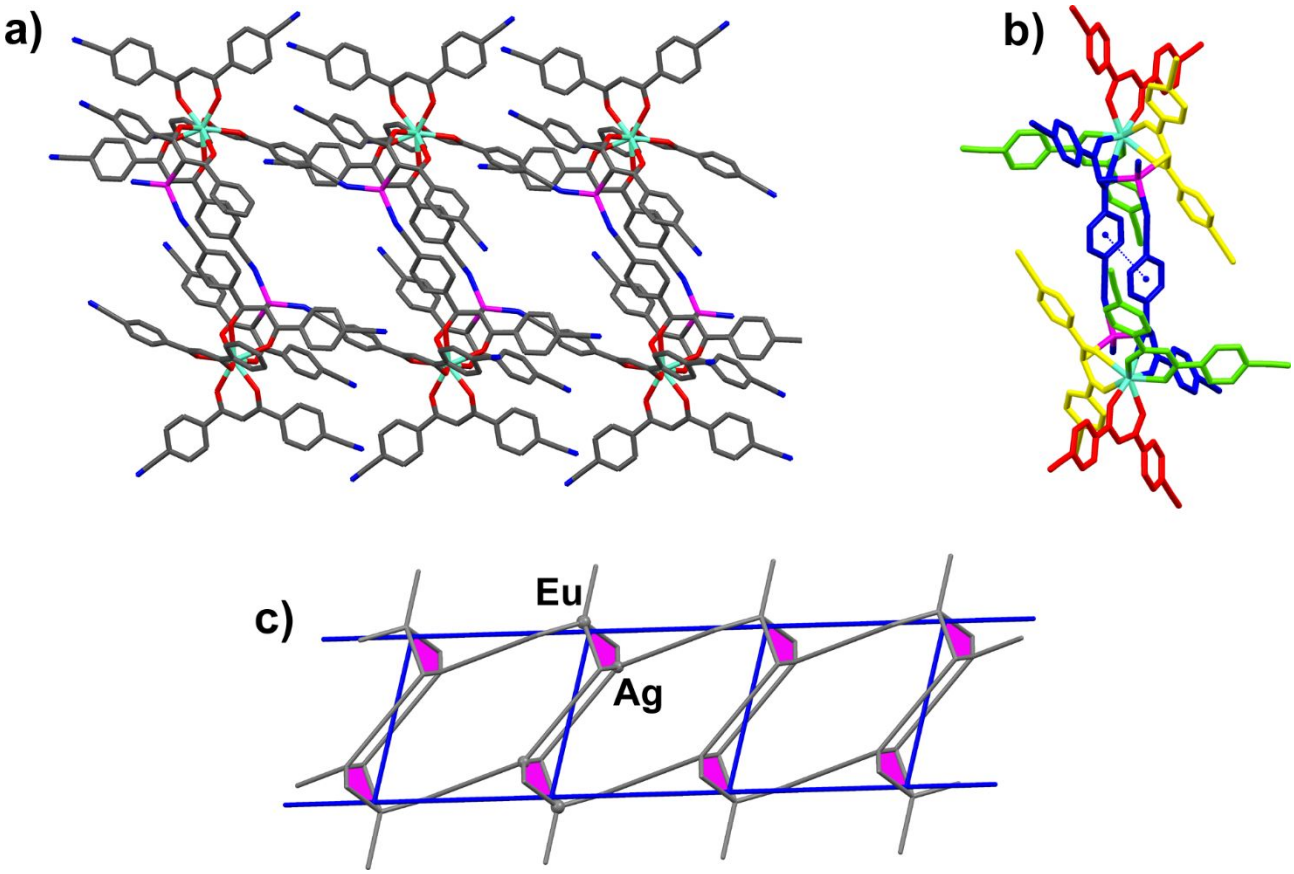

Figure 3. Views of a single molecular ladder motif in **2a**, hydrogen atoms have been omitted for clarity. a) Front view and b) lateral view of the ladder running along **b**, showing the π-π interaction reinforcing the rungs of the ladder. c) Simplified representations of the ladder obtained considering europium and silver atoms as nodes (in grey, the silver pincer is highlighted in pink) and considering the whole SBUs as nodes (in blue).

The main structural features concern the interactions of the silver ions with the Ln metalloligands and the role of the β-diketonate ligands in the networking process. In this structure only one silver-SBU (of the type previously described) *per* ML is observed. Out of the four β-diketonate ligands of a ML two are involved in the silver-SBU, with Ag–C bonds in the range 2.447(4)–2.486(6) Å. Two adjacent SBUs interconnect *via* mutual exchange of one CN–Ag link using one of their two diketonate ligands (Figure 3a). These double-bridged centrosymmetric pairs form the rungs of the ladder-like ~~polymeric~~ motif. The rungs show strong reinforcing π-π interactions between the phenyl rings of the ligands (for the two phenyl rings the center-to-center distance is 3.901(10) Å and the stacking distance is 3.35 (12) Å) (Figure 3b). Of the two diketonate ligands not involved in the formation of the SBU, one, outward oriented with respect to the ladder, remains dangling or "free", while the other employs a CN group to bind a silver ion on a nearest neighboring rung, thus forming the rails of the ladder.
The four diketonate ligands belonging to a ML differ in their interactions with the silver cations: the first one uses the central carbon atom and one CN group, the second one only the central carbon atom, the third one a CN group, and the fourth one is completely non-interacting. Surprisingly, only two CN donor groups *per* ML are involved in bonds to silver, one to build the rails and the other the rungs of the ladder motif.
Each Ag atom is therefore four-connected, with an AgC_2N_2 environment of distorted tetrahedral geometry; the Ag–N bond lengths are in the range 2.257(5)–2.284(6) Å.

As already observed for the metalloligands **1a**–**1d**, the six-membered chelate rings are folded along the O···O vector with dihedral angles between the EuO_2 plane and the plane of the ligand (defined by the two oxygen atoms and the γ-carbon atom) in the range 12.5(3)– 26.5(3)°.

The major differences are expected between the two diketonate ligands wrapping the silver atom [with a C–Ag–C angle of 122.3(2)°] with respect to the other two ligands, as a consequence of the partial re-hybridization of the central carbon atom from sp^2 to sp^3 and the consequent decrease of the π-electron delocalization: indeed, the C–C–C bond angles are smaller [120.4(6) and 120.1(6)° *vs* 123.6(7) and 123.6(8)°] and the C–C bond lengths longer [range 1.423(9)–1.444(9) Å *vs* range 1.393(9)–1.415(10) Å].
The ladders are packed in a parallel arrangement, running along the ***b*** direction.

3.2.2 2D coordination networks [Ln(L^1)$_4$Ag] (3a–3c)

On performing the reactions leading to the family **2a**–**2d** in a different solvent system, replacing ethanol with water, the new family [Ln(L^1)$_4$Ag] [Ln = Eu, La, and Nd (**3a**–**3c**)] can be isolated. Crystals of these species are very unstable and accurate structural determinations could not be accomplished; nevertheless, they were shown to be isostructural by comparing their PXRD patterns (Figure S5). After many attempts, single-crystal diffraction analysis was possible for a sample of **3b**, even if the low quality of the data collected allowed to refine the skeleton of the framework only (Table S7). This partial result suffices to establish the supramolecular isomeric relationship existing between the families **2** and **3**, sharing the network composition [Ln(L^1)$_4$Ag]. The structure is illustrated in the top row of Figure 4 and consists of slightly undulated 2D layers with large windows. As for compounds of the family **2**, also in these species **3a**–**3c** we observe the presence of only one SBU *per* ML (Figure 4a–b). All the CN groups of the two diketonate ligands involved in the formation of the SBU with the silver atom remain free, while each of the other two diketonates of the Ln-ML uses one CN group to bind the silver ions of two lateral SBUs. Overall there are two distinct types of diketonates: a pair that uses only the central carbon atom to bind silver, and a second pair that uses one CN donor group. Therefore, also in this case only two CN groups of the ML (out of eight) are employed for networking.
The topology of the layers can be rationalized in two different ways: assuming as nodes the entire SBUs we can idealize these single-edged windows as squares, giving a 4^4-**sql** topology (as shown in red in Figure 4c), while using both silver and lanthanide atoms as distinct nodes we obtain a honeycomb network (6^3-**hcb**, as shown in blue in Figure 4c).
The main difference between the structures of these supramolecular isomers (families **2** and **3**) are related to the orientation of the SBUs in the network (compare Figure 3c and 4b). While sequences of SBUs oriented in alternate directions lead to the 1D ladder, sequences of SBUs oriented all in the same direction lead to the 2D network **3**. This latter orientation results in a polar direction in the layers (the polar axis running along **b**), with adjacent layers showing opposite polarity. Indeed, these layers are stacked down **c** with an ABAB sequence (Figure S13). The absence of counter-ions and the slight displacement of the stacking layers ~~in this structure~~ generate large 1D channels along the stacking direction, that may be the reason of the instability of **3b**.

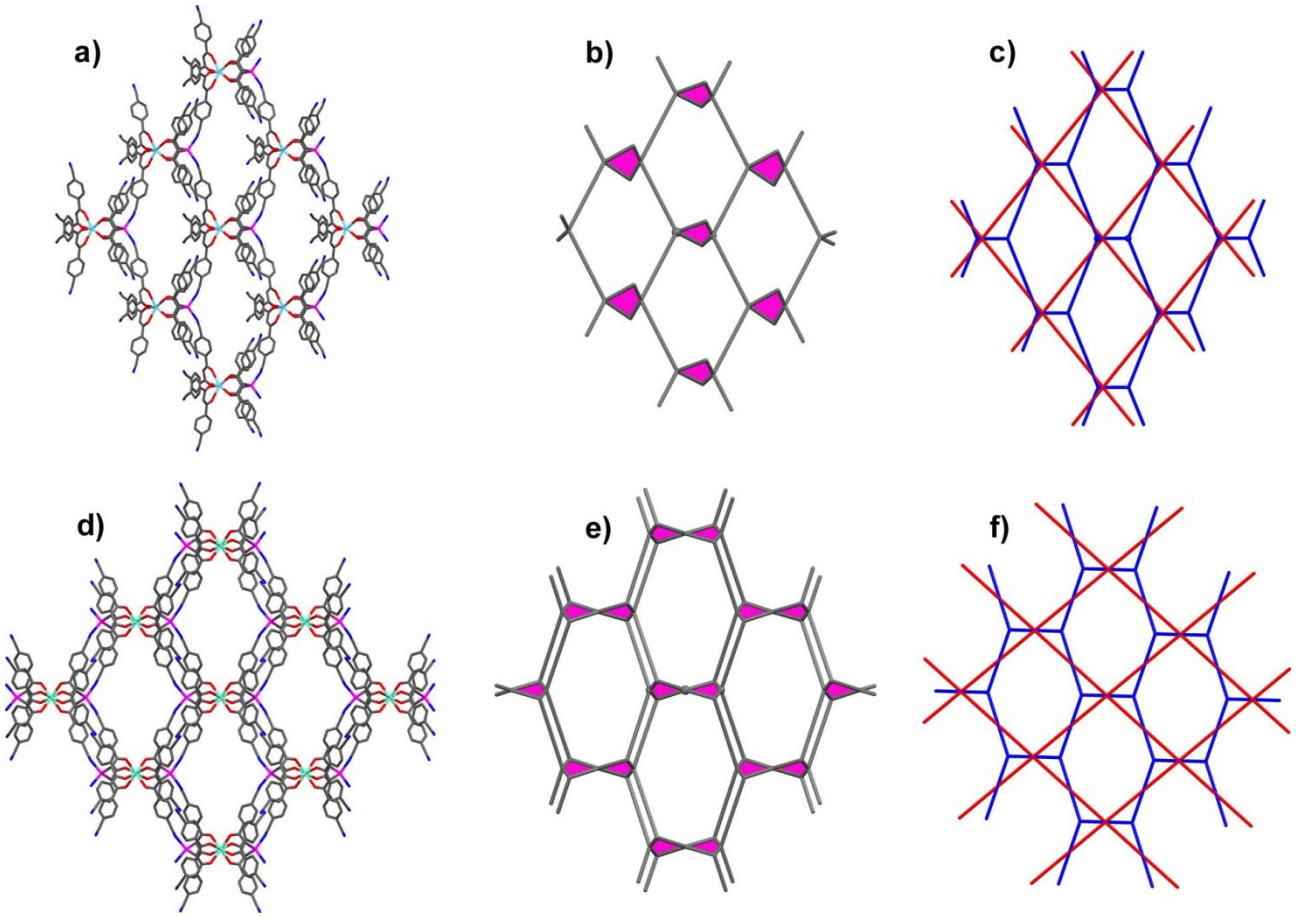

Figure 4. A comparison of the two families of 2D polymeric structures (**3** in the upper row and **4** in the lower row). In the left column (a and d) the molecular drawings; in the middle column (b and e) the corresponding schematic drawings, in which the different types of SBU has been highlighted in pink; and in the right column (c and f) the simplified networks obtained by considering the silver and lanthanide atoms as nodes (in blue) or the whole SBUs as nodes (in red).

3.2.3 2D coordination networks $[Ln(L^1)_4Ag_2]X$ (4a–4f)

The reactions of all ~~the~~ Ln-MLs with different silver salts (hexafluorophosphate, perclorate, and triflate) in a stoichiometric ratio of 1:2 in CH_2Cl_2/EtOH (1:1) generate the species $[Ln(L^1)_4Ag_2]X$ [Ln = Eu, X = PF_6^-, $CF_3SO_3^-$, ClO_4^- (**4a**–**4c**); Ln = Tb, Nd, La, X = PF_6^- (**4d**–**4f**)]. Their structure is illustrated in the bottom row of Figure 4. As for the synthesis of the previous species, the structure determining factors are the stoichiometric ratio ML/Ag of 1:2 and the solvent system emploied. The nature of the counter-anion of the silver salt seems not to influence the outcome of the reactions. As a consequence, we believe that this family of polymers could include other species with anions of similar shape, such as BF_4^-, AsF_6^-, and SbF_6^-. All the crystals belong to the orthorhombic system, space group *Pnca*, and their structure contains a 2D network of squares, using the whole SBUs as nodes (Figure 4f, in red) or hexagonal double-edged meshes, using the metal atoms as nodes (Figure 4f, in blue). This framework is unique, being characterized by the presence of two silver-pincer SBUs *per* ML (Scheme 2).

In this structure, all the four diketonate ligands of the Ln-ML play the same role, *i.e.* they form each an Ag–C bond *via* the central carbon atom and use one of their two CN groups to bind the silver ion of a lateral SBU. Overall, four CN groups (out of eight) are employed by each ML for networking. All the edges of the square windows are reinforced by π-π interactions between phenyl rings [for the two phenyl rings the centre-to-centre distance is 4.459(13) Å and the angle between the phenyl rings is 3.37(12)°]. The layers in family **4** are stacked with an ABAB sequence along **a** and the disordered counter-anions are located in the channels running in the same direction (Figure S14). The double edges and the disordered

anions obstruct the 1D channels running along the stacking direction, creating isolated voids that add up to 19% of the cell volume.

3.2.4 2D coordination network [La(L^1)$_4$(H_2O)Ag] (5)

Only with the lanthanum metalloligand **1b** a fourth type of polymeric array can be obtained, having formula [La(L^1)$_4$(H_2O)Ag] (**5**). Bulk microcrystalline powders of this species are obtained from the same reaction system leading to **3b** by fast addition of an aqueous silver solution to the lanthanum metalloligand **1b** dissolved in acetonitrile. Single crystals of **5** are grown slowly, in about one month, after the disappearance of the crystals of **3b** initially formed (a solvent mediated process).

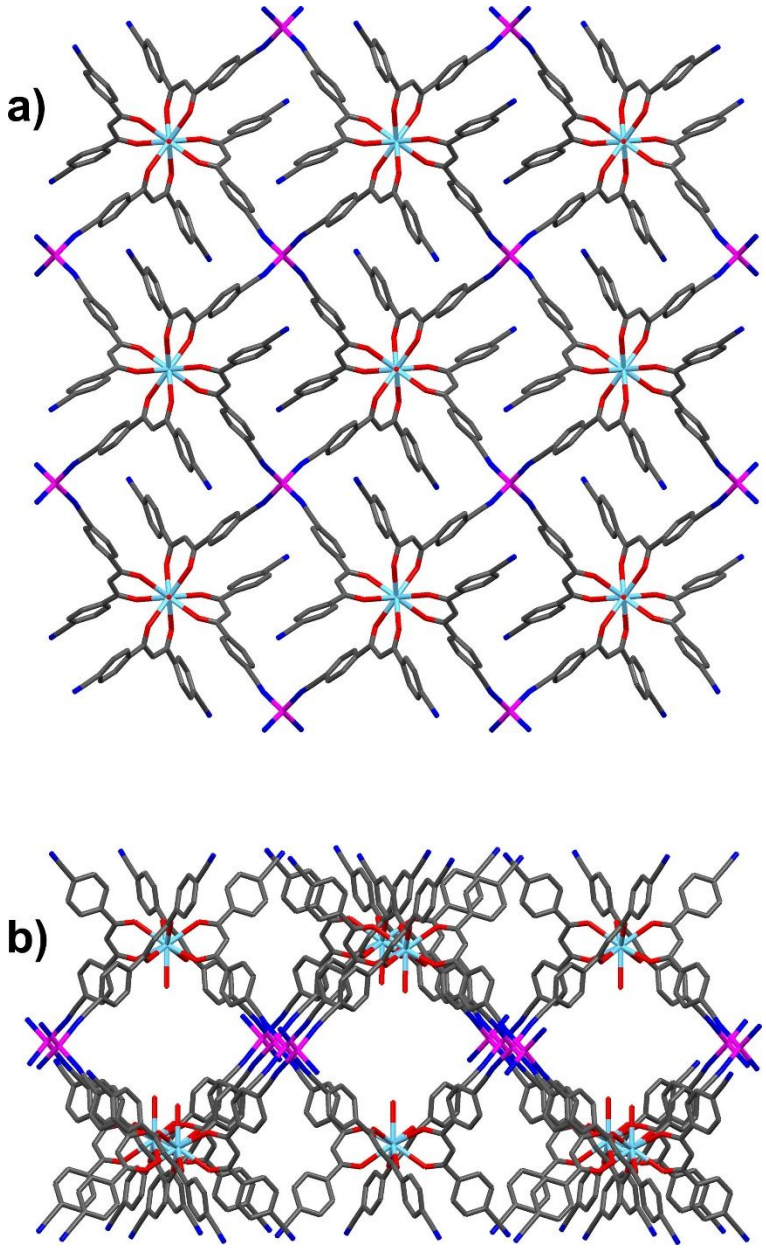

Figure 5. Two views of a single molecular layer of compound **5**, down **c** (top) and [110] (bottom).

The new species shows again a 2D polymeric structure, in which however no silver pincer-like SBUs are present and only the CN groups (4 groups *per* ML) are involved in the coordination to the silver cations (Figure 5). Since this structure can be obtained only with the La metalloligand, *i.e.* the species containing the metal with the largest ionic radius, this feature is probably of relevance in driving this

structural type formation. Indeed, the lanthanum cation is 9-coordinated, with an additional water molecule in the inner coordination sphere [La–O 2.712(8) Å], and adopt a monocapped square-antiprismatic geometry (*SAPRS*-9).

The topological simplification of the 2D network **5**, considering the lanthanum and silver atoms as nodes, gives a square layer 4^4-**sql** with single edges (Figure 6a). However, the structural type is related to that of the red polymorph of PbO (litharge) since it is not flat and the two types of 4-connected nodes are different: the La nodes show a square pyramidal geometry, while the Ag nodes are (slightly) distorted tetrahedral [N–Ag–N angles 101.2(4) and 113.78(19)°]. As clearly evidenced by the simplified representation of the network, the layers are strongly puckered and stacked with interdigitation in an *AAA* sequence along **c**. A remarkable resemblance of this network with an egg tray can be noticed (Figure 6b).

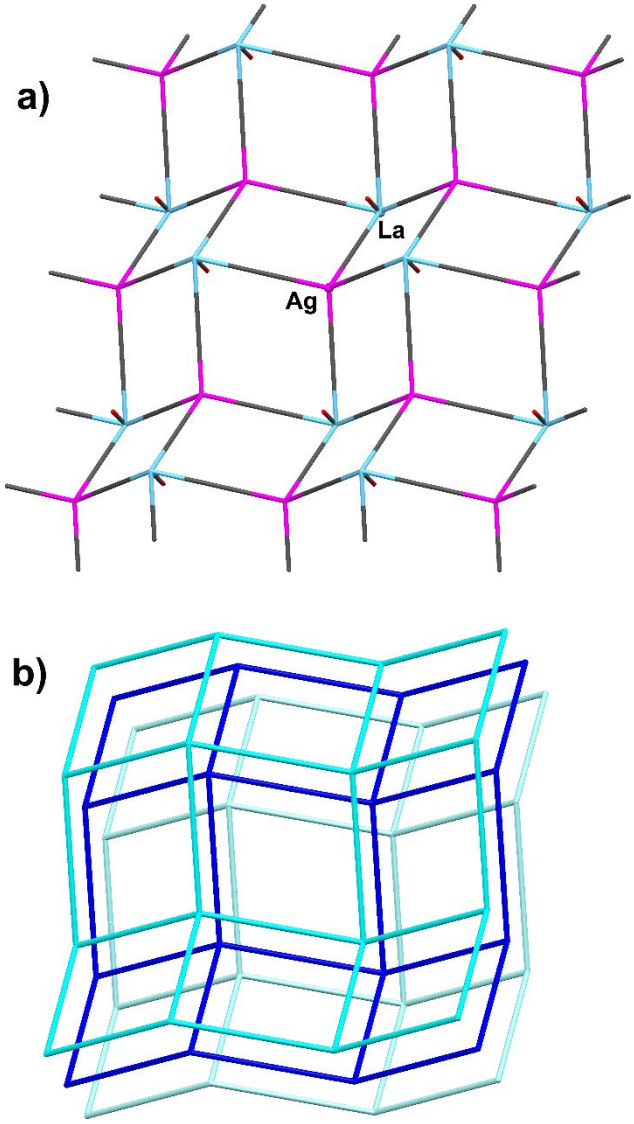

Figure 6. Views of the simplified network of **5** obtained by considering the metal atoms as nodes (lanthanum in blue and silver in pink). In a) a single layer is presented, showing the position of the water molecules coordinated to the lanthanum ions. In b) the staking of the egg-tray like layers along **c** is evidenced.

Interestingly, a side view of the layer shows that the uncoordinated CN groups are all oriented outwards the two surfaces of the layers (Figure 5b) while, on the other hand, all the La-water vectors are oriented towards the middle section of the layer. The exo-oriented donor groups could in principle allow interactions of the layers with external metal ions. The two types of nitrile groups (coordinated

to the silver ions and free), at variance from what observed in all the previously presented complexes, are clearly distinguishable in the IR spectra.

3.3 Luminescence properties

We studied the photophysical properties of the ligands (HL^1 and HL^2) and of their complexes in dichloromethane solution and in the solid state, and of the coordination polymers in the solid state only. The most relevant data are gathered in Table 1. The absorption spectra of the free ligands and of the corresponding europium metalloligands are reported in Figure 7.

HL^1 presents absorption maxima at 255 and 352 nm, and a large and not structured fluorescence band centered at 405 nm at room temperature (both in solution and in the solid state) with a low emission quantum yield ($< 10^{-4}$). Because of its energy and excited state lifetime, this band can be attributed to a spin allowed fluorescence transition. HL^2 presents very similar characteristics but with slightly higher energies in absorption and emission that falls at 400 nm in solution, with a quantum yield similar to that of HL^1.

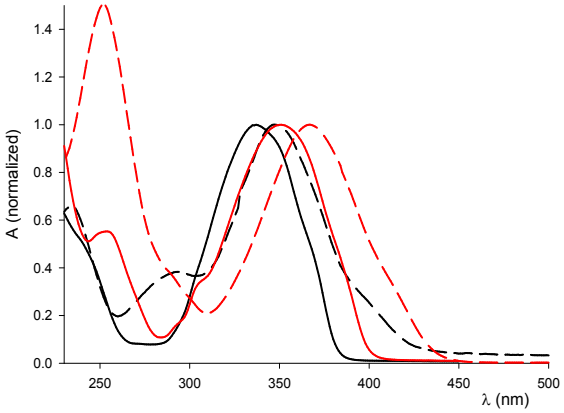

Figure 7. Absorption spectra in CH_2Cl_2 of the free ligands (solid lines) HL^1 (red) and HL^2 (black) and the corresponding europium complexes (dot lines) $NEt_4[Eu(L^1)_4]$ (**1a**) (red) and $NEt_4[Eu(L^2)_4]$ (**1e**) (black). To facilitate shape comparison, all the spectra are normalized on the maximum of the lower absorption band.

All the monomeric lanthanide complexes $NEt_4[Ln(L^1)_4]$ were characterized both at room temperature and at 77 K in dichloromethane solution. Due to their low intrinsic absorption, lanthanide ions can present a high brightness only if an efficient antenna effect through the light excitation of suitable ligands and an efficient energy transfer process to the metal-centered states of the metal ions can be obtained. A first parameter to be observed is thus the energy of the ligand- centered states in the complexes. For this purpose, we carefully characterized the lanthanum complex **1b**, since La^{3+}, presenting the close shell electronic configuration of xenon, does not usually have metal-centered (MC) emission bands.[56] The absorption spectrum of the complex presents the features of the ligand absorption profile but with the band at lower wavelength shifted to 365 nm, as expected upon metal complexation. It is important to mention that the absorption spectrum of **1b** is superimposable with those of all the other complexes with HL^1, indicating that the ligand experiences similar complexation environments in all the **1a**–**1d** species (Figure S15). The emission spectrum of **1b** at room temperature presents a broad fluorescence band at circa 380 nm with a lifetime of 2 ns, while at 77 K it shows also a lower-energy (555 nm) longer-lived (2.2 ms) band attributable to a ^{3}LC transition (Figure S16). It is important to note that, according to these data, the ^{3}LC state (19250 cm^{-1}) is lower in energy than the MC $^5D_4$ state of the Tb^{3+} ion, suggesting that the ligand HL^1 is not able to sensitize the typical MC emission of this ion. In agreement with this consideration, **1d** does not present any typical MC emission in solution, not even at low temperature.

Table 1. Photophysical properties of the ligands, the metalloligands, and the heterometallic coordination networks. [a]

compound	absorption maxima (nm)	emission maxima (nm)	emission lifetime (μs)
HL^1	255, 352	405	3 ns
$NEt_4[Eu(L^1)_4]$ (**1a**)	252, 368	615 (615)	41, 21_{pw} (430)
1D-$[Eu(L^1)_4Ag]$ (**2a**)		615_{pw}	20_{pw}
2D-$[Eu(L^1)_4Ag]$ (**3a**)		615_{pw}	15_{pw}
2D-$[Eu(L^1)_4Ag_2]PF_6$ (**4a**)		615_{pw}	20_{pw}
$NEt_4[La(L^1)_4]$ (**1b**)	256, 365	380[b] (555)	2 ns[b] (2.2 ms)
$NEt_4[Nd(L^1)_4]$ (**1c**)	256, 367	893, 1065	–[c]
1D-$[Nd(L^1)_4Ag]$ (**2c**)		894_{pw}, 1070_{pw}	–[c]
2D-$[Nd(L^1)_4Ag]$ (**3c**)		894_{pw}, 1070_{pw}	–[c]
$NEt_4[Tb(L^1)_4]$ (**1d**)	256, 367	390[b]	2 ns[b]
HL^2	243, 338	400	5 ns
$NEt_4[Eu(L^2)_4]$ (**1e**)	290, 350	615	140, 480_{pw}
$NEt_4[Nd(L^2)_4]$ (**1f**)	255, 367	890, 1064	–[c]

[a] All the values determined in dichloromethane solution at room temperature, apart from the ones in round brackets, determined at 77 K, and the ones with the subscript "pw", measured for the microcrystalline powders. [b] Data relative to the LC emission. [c] Not possible to measure with our instrumentation.

The emission spectrum of compound **1a** reveals the typical MC bands of the europium ion (Figure 8) and it is possible to observe the $^0D_5 \rightarrow {}^7F_J$ transitions with J from 0 to 4. The presence of the forbidden $^0D_5 \rightarrow {}^7F_0$ and $^0D_5 \rightarrow {}^7F_3$ transitions and, above all, the high value of the ratio between the $^0D_5 \rightarrow {}^7F_2$ and $^0D_5 \rightarrow {}^7F_1$ intensities are in line with a low symmetry environment of the Eu^{3+} ion, lacking an inversion center, in agreement with the geometry observed in the crystal structure (Figure 1). The energy of the ^{3}LC transition is, in this case, compatible with a good energy transfer from the ligand to the metal center.

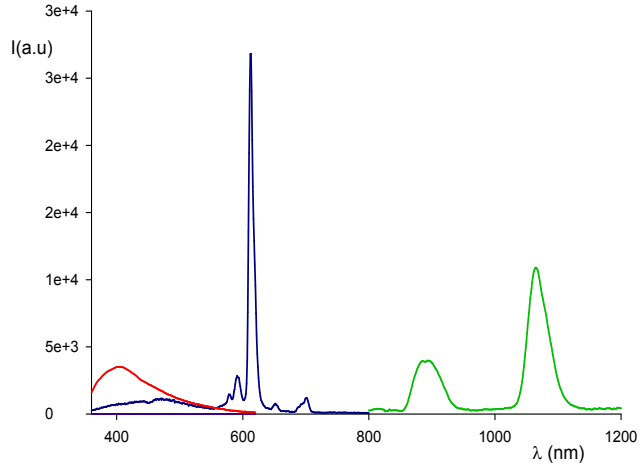

Figure 8. Emission spectra in CH_2Cl_2 at r.t. of the free ligand HL^1 (red, λ_{ex} 320 nm) and the complexes $NEt_4[Eu(L^1)_4]$ (**1a**) (black, λ_{ex} 340 nm) and $NEt_4[Nd(L^1)_4]$ (**1c**) (green, λ_{ex} 370 nm).

However, the measurements of its lifetime (Table 1) give quite low values not in line with what expected for similar compounds (lifetimes in the range of hundreds of microseconds), evidencing the presence of favorable non-radiative deactivation pathways. The energy of the MC state is close to the one of the ^{3}LC transition, so that the sensitization of the MC state is possible but with the establishment of a thermally activated equilibrium between the two states. The ten-fold increase of the emission lifetime observed at low temperature (77 K) supports this assumption. The neodymium complex **1c** is also efficiently populated by the ligand and presents the typical IR bands at 893 and 1065 nm with an interesting emission quantum yield of circa 2%.

The two $NEt_4[Ln(L^2)_4]$ complexes **1e** and **1f** show luminescence spectra very similar to those observed for their L^1 homologues, but with a longer lifetime (Table 1, Figure S17), probably due to the higher energy of the ^{3}LC state in this case, a condition that would shift the above mentioned equilibrium in favor of the europium MC state.

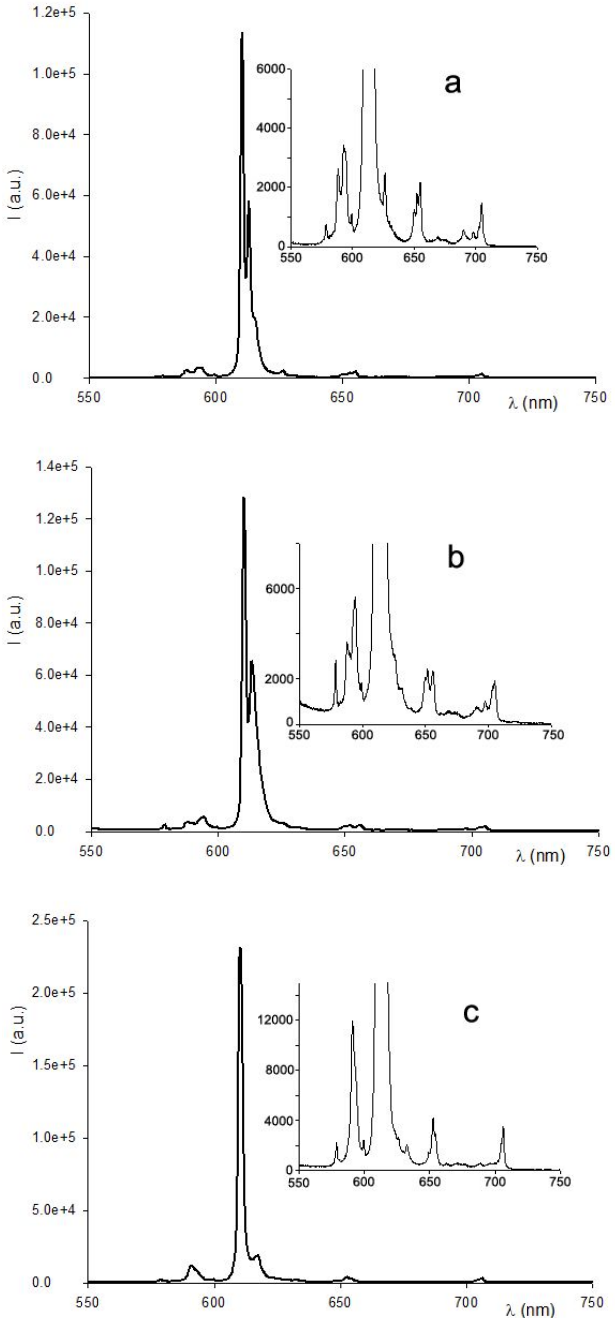

Figure 9. Emission spectra at r.t. of the solid powders of (a) $[Eu(L^1)_4Ag]$ (**2a**), (b) $[Eu(L^1)_4Ag]$ (**3a**), and (c) $[Eu(L^1)_4Ag_2]PF_6$ (**4a**). Insets: enlarged lower intensity peaks.

Due to the lack of luminescence of the lanthanum and terbium complexes, it was possible to characterize only the 1D and 2D polymers containing europium (**2a**, **3a**, and **4a**, Figure 9) and neodymium (**2c** and **3c**). As a general remark, results obtained for the microcrystalline powders and the single crystals (data not shown) of the same species were always identical. A comparison of the data obtained for the metalloligands and for the corresponding silver-lanthanide coordination networks allows to observe that the presence of the silver centers did not significantly change the photophysical behavior of this species. This means that the presence of silver pincer-like secondary building units does not add other efficient non-radiative deactivation pathways for the excited states. It has also to be mentioned that the series of 2D structures containing europium and bearing different counter anions (**4a**–**4c**) presents again analogous characteristics and, for this reason, the corresponding data are not reported in Table 1.

4 Conclusions

The construction of heterometallic metal-organic framework is generally a difficult task to be accomplished due to the propensity of a given donor group to better coordinate to a specific metal. One of the strategies employed to attain this result involves the use of asymmetric ligands in which different coordinating groups can be directed towards different metal centers. The stepwise metalloligand approach represents a valid alternative that, in addition, allows to exert a better control on the topology of the assembled network ~~prepared~~. However, this stepwise approach has not been yet fully exploited in the case of HMOF containing lanthanides metalloligands.

In this work we explored the use of two new tetrakis-chelate Ln-MLs, containing the 1,3-disubstituted diketonate ligands HL^1 and HL^2, in order to prepare HMOFs by reaction with silver cations. It was found that this approach gives good results only using the metalloligands based on the 4-cyanophenyl-substituted diketonate HL^1, obtaining different families of 1D and 2D HMOFs. On the other hand, the lability in solution of the metalloligands based on the 4-pyridyl-substituted diketonate HL^2 prevents their networking with silver cations.

The structures of the monomeric building blocks and those of four families of lanthanide-silver heterometallic networks has been described, allowing to point out some general features of their synthetic strategy and to ascertain the coordination ability of the starting lanthanide metalloligands.

In particular, we found that both the Ln-to-Ag stoichiometric ratio and the solvent employed in the syntheses proved to be crucial in determining the nature of the structures assembled. We also observed that the coordination capabilities of the Ln-MLs could not be fully exploited, due to the high number of cyano groups *per* ML and to the additional formation of the silver pincer-like SBUs that induce a deformation in the coordination environment of the metal atoms. Both these factors lead to the preferential formation of 1D and 2D networks over 3D ones. Nevertheless, some of the prepared materials are porous and in one of the isolated families (**4**) the presence of about 20% of free volume can be estimated from the crystallographic data.

The photophysical characterization of the ligands and the metalloligands evidenced that lanthanum and terbium complexes are not emissive while the europium ones present quite low intensities and lifetimes due to similar energies of the MC and ^{3}LC states that give rise to a thermally activated equilibrium. On the other side, the sensitization of ~~the~~ neodimium complexes is very efficient. The heterometallic coordination networks have similar photophysical behaviour evidencing that, both in 1D and 2D structures, the presence of silver ions does not add other efficient non-radiative deactivation pathways.

The results here presented point out some of the features of the lanthanide metalloligands and of their interaction with silver cations that could be fruitfully employed in the development of new HMOFs with tailored structures and properties.

Supporting Information
The Supporting Information is available free of charge on the ACS Publications website.
TGA plots; X-ray powder diffraction patterns; representations of molecular and crystal structures; absorption and emission spectra; tables of crystallographic data.

Author Information
Corresponding Author
*E-mail: lucia.carlucci@unimi.it
ORCID
Pierluigi Mercandelli: 0000-0002-9473-6734
Luca Prodi: 0000-0002-1630-8291
Massimo Sgarzi: 0000-0001-6938-3909
Nelsi Zaccheroni: 0000-0002-4517-6611
Lucia Carlucci: 0000-0001-5856-5280

Notes
The authors declare no competing financial interest.

Acknowledgments
We gratefully acknowledge financial support from the Fondazione Cariplo (grant no: 2012–0921).

References

(1) Yaghi, O. M.; O'Keeffe, M.; Ockwig, N. W.; Chae, H. K; Eddaoudi, M.; Kim, J. Reticular Synthesis and the Design of New Materials. *Nature* **2003**, *423*, 705–714.
(2) Kalmutzki, M. J.; Hanikel, N.; Yaghi, O. M. Secondary Building Units as the Turning Point in the Development of the Reticular Chemistry of MOFs. *Sci. Adv.* **2018**, *4*, eaat9180.
(3) Kim, D.; Coskun, A. Template-Directed Approach Towards the Realization of Ordered Heterogeneity in Bimetallic Metal-Organic Frameworks. *Angew. Chem. Int. Ed.* **2017**, 56, 5071–5076.
(4) Falcaro, P.; Ricco, R.; Doherty, C. M.; Liang, K.; Hill, A. J.; Styles, M. J. MOF Positioning Technology and Device Fabrication. *Chem. Soc. Rev.* **2014**, *43*, 5513–5560.
(5) Kumar, P.; Pournara, A.; Kim, K.-H.; Bansal, V.; Rapti, S.; Manos, M. J. Metal-Organic Frameworks: Challenges and Opportunities for Ion-Exchange/Sorption Applications. *Progress in Materials Science* **2017,** *86*, 25–74.
(6) Jiao, L.; Wang, Y.; Jiang, H.-L.; Xu, Q. Metal-Organic Frameworks as Platforms for Catalytic Applications. *Adv. Mater.* **2018**, *30*, 1703663.
(7) Zhang, Y.; Yuan, S.; Day, G.; Wang, X.; Yang, X.; Zhou, H.-C. Luminescent Sensors Based on Metal-Organic Frameworks. *Coord. Chem. Rev.* **2018**, *354*, 28–45.
(8) Espallargas, G. M.; Coronado, E. Magnetic Functionalities in MOFs: From the Framework to the Pore. *Chem. Soc. Rev.* **2018**, *47*, 533–557.
(9) Lustig, W. P.; Li, J. Luminescent Metal-Organic Frameworks and Coordination Polymers as Alternative Phosphors for Energy Efficient Lighting Devices. *Coord. Chem. Rev.* **2018**, *373*, 116–147.
(10) Cui, Y.; Zhang, J.; He, H.; Qian, G. Photonic Functional Metal-Organic Frameworks. *Chem. Soc. Rev.* **2018**, *47*, 5740–5785.
(11) Gas adsorption Lin, R.-B.; Xiang, S.; Xing, H.; Zhou, W.; Chen B. Exploration of porous metal–organic frameworks for gas separation and purification Gas-adsorption. *Coord. Chem. Rev.* **2019**, *378*, 87–103.
(12) Zhao, X.; Wang, Y.; Li, D.-S.; Bu, X.; Fen, P. Metal-Organic Frameworks for Separation. *Adv. Mater*. **2018**, *30*, 705189.

(13) Chen, C.-X.; Wei, Z.-W.; Jiang, J.-J.; Zheng, S.-P.; Wang, H.-P.; Qiu, Q.-F.; Cao, C.-C.; Fenske, D.; Su, C.-Y. Dynamic Spacer Installation for Multirole Metal-Organic Frameworks: A New Direction Toward Multifunctional MOFs Achieving Ultrahigh Methane Storage Working Capacity. *J. Am. Chem. Soc*. **2017**, *139*, 6034−6037.
(14) Cui, Y.; Yue, Y.; Qian, G.; Chen, B. Luminescent Functional Metal-Organic Frameworks. *Chem. Rev*. **2012**, *112*, 1126–1162.
(15) Wu, Z.-L.; Dong, J.; Ni, W.-Y.; Zhang, B.-W.; Cui, J.-Z.; Zhao, B. Unique Chiral Interpenetrating d-f Heterometallic MOFs as Luminescent Sensors. *Inorg. Chem*. **2015**, *54*, 5266−5272.
(16) Das, M. C.; Xiang, S.; Zhang, Z.; Chen, B. Functional Mixed Metal-Organic Frameworks with Metalloligands. *Angew. Chem. Int. Ed*. **2011**, *50*, 10510–10520.
(17) Kumar, G.; Gupta, R. Molecularly Designed Architectures – The Metalloligand Way. *Chem. Soc. Rev.* **2013**, *42*, 9403–9453.
(18) Garibay, S. J.; Stork, J. R.; Cohen, S. M. The Use of Metalloligands in Metal-Organic Frameworks. *Prog. Inorg. Chem*. **2009**, *56*, 335−378.
(19) Srivastava, S.; Gupta, R. Metalloligands to Material: Design Strategies and Network Topologies. *CrystEngComm* **2016**, *18*, 9185–9208.
(20) Sørensen, M. A.; Weihe, H.; Vinum, M. G.; Mortensen, J. S.; Doerrer, L. H.; Bendix, J. Imposing High-Symmetry and Tuneable Geometry on Lanthanide Centres with Chelating Pt and Pd Metalloligands. *Chem. Sci*. **2017**, *8*, 3566–3575.
(21) Sakamoto. M.; Manseki. K.; Okawa H. d-f Heteronuclear Complexes: Synthesis, Structures and Physicochemical Aspects. *Coord. Chem. Rev*. **2001**, *219*, 379–414.
(22) Liu, K; Shi, W.; Cheng, P. Toward Heterometallic Single-Molecule Magnets: Synthetic Strategy, Structures and Properties of 3d-4f Discrete Complexes. *Coord. Chem. Rev*. **2015**, 289, 74–122.
(23) Zhou, Y.; Hong, M.; Wu, X. Lanthanide-Transition Metal Coordination Polymers Based on Multiple N- and O-Donor Ligand. *Chem. Commun*. **2006**, 135–143.
(24) Peng, G.; Qiu, Y.-C.; Liu, Z.-H.; Liu, B.; Deng, H. Spontaneous Assembly of d-f Coordination Frameworks: Syntheses, Structures, and Photoluminescence. *Cryst. Growth Des*. **2010**, *10*, 114–121.
(25) Feng, X.; Feng, Y.; Guo, N.; Sun, Y.; Zhang, T.; Ma, L.; Wang, L. Series d−f Heteronuclear Metal-Organic Frameworks: Color Tunability and Luminescent Probe with Switchable Properties. *Inorg. Chem*. **2017**, *56*, 1713−1721.
(26) Chandler, B. D.; Yu, J. O.; Cramb, D. T.; Shimizu, G. K. H. Series of Lanthanide-Alkali Metal-Organic Frameworks Exhibiting Luminescence and Permanent Microporosity. *Chem. Mater.* **2007,** *19,* 4467−4473.
(27) Chandler, B. D.; Cramb, D. T.; Shimizu, G. K. H. Microporous Metal-Organic Frameworks Formed in a Stepwise Manner from Luminescent Building Blocks. *J. Am. Chem. Soc.* **2006**, 128, 10403−10412.
(28) Chandler, B. D.; Coté, A. P.; Cramb, D. T.; Hill, J. M.; Shimizu, G. K. H. A Sponge-Like Luminescent Coordination Framework *Via* an Aufbau Approach. *Chem. Commun.* **2002**, 1900−1901.
(29) Liu, Y.; Pan, M.; Yang, Q.-Y.; Fu, L.; Li, K.; Wei, S.-C.; Su, C.-Y. Dual-Emission from a Single-Phase Eu-Ag Metal-Organic Framework: An Alternative Way to Get White-Light Phosphor. *Chem. Mater.* **2012**, *24*, 1954−1960.
(30) Ma, J.-X.; Huang, X.-F.; Song, X.-Q.; Liu, W.-S. Assembly of Framework-Isomeric 4d−4f Heterometallic Metal-Organic Frameworks with Neutral/Anionic Micropores and Guest-Tuned Luminescence Properties. *Chem. Eur. J.* **2013**, 19, 3590−3595.
(31) Huang, X.-F.; Ma, J.-X.; Liu, W.-S. Lanthanide Metalloligand Strategy Toward d-f Heterometallic Metal-Organic Frameworks: Magnetism and Symmetric-Dependent Luminescent Properties. *Inorg. Chem.* **2014**, 53, 5922−5930.

(32) Ma, J.-X.; Guo, J.; Wang, H.; Li, B.; Yang, T.; Chen, B. Microporous Lanthanide Metal-Organic Framework Constructed from Lanthanide Metalloligand for Selective Separation of C_2H_2/CO_2 and C_2H_2/CH_4 at Room Temperature. *Inorg. Chem*. **2017**, *56*, 7145−7150.
(33) Qiu, J.-Z.; Wang, L.-F.; Chen, Y.-C.; Zhang, Z.-M.; Li, Q.-W.; Tong, M.-L. Magnetocaloric Properties of Heterometallic 3d-Gd Complexes Based on the $[Gd(ODA)_3]^{3-}$ Metalloligand. *Chem. Eur. J*. **2016**, *22*, 802−808.
(34) Niu, Z.; Ma, J.-G.; Shi, W.; Cheng, P. Water Molecule-Driven Reversible Single-Crystal to Single-Crystal Transformation of a Multi-Metallic Coordination Polymer with Controllable Metal Ion Movement. *Chem. Commun.,* **2014**, 50, 1839−1841.
(35) Carlucci, L.; Ciani, G.; Maggini, S.; Proserpio, D. M.; Visconti, M. Heterometallic Modular Metal-Organic 3D Frameworks Assembled via New Tris-β-Diketonate Metalloligands: Nanoporous Materials for Anion Exchange and Scaffolding of Selected Anionic Guests. *Chem. Eur. J.* **2010**, 16, 12328−12341.
(36) Carlucci, L.; Ciani, G.; Proserpio, D. M.; Visconti, M. The Novel Metalloligand $[Fe(bppd)_3]$ (bppd = 1,3-Bis(4-pyridyl)-1,3-propanedionate) for the Crystal Engineering of Heterometallic Coordination Networks with Different Silver Salts. Anionic Control of the Structures. *CrystEngComm* **2011**, 13, 5891−5902.
(37) Montalti, M.; Credi, A.; Prodi, L.; Gandolfi, M. T. *Handbook of Photochemistry* (3rd ed.); Taylor & Francis: 2006, pp. 561–581.
(38) Sheldrick, G. M. *SADABS: Software for Empirical Absorption Correction*; Universität Göttingen, Institute für Anorganische Chemie, Göttingen, Germany, 1999−2012.
(39) Altomare, A.; Burla, M. C.; Camalli, M.; Cascarano, G. L.; Giacovazzo, C.; Guagliardi, A.; Moliterni, A. G. G.; Polidori, G.; Spagna, R. SIR97: A New Tool for Crystal Structure Determination and Refinement. *J. Appl. Crystallogr.* **1999**, *32*, 115–119.
(40) Sheldrick, G. M. Crystal Structure Refinement with SHELXL. *Acta Crystallogr., Sect. C: Struct. Chem.* **2015**, *71*, 3–8.
(41) Farrugia, L. J. WinGX and ORTEP for Windows: An Update. *J. Appl. Crystallogr.* **2012**, *45*, 849–854.
(42) Spek, A. J. PLATON SQUEEZE: A Tool for the Calculation of the Disordered Solvent Contribution to the Calculated Structure Factors. *Acta Crystallogr., Sect. C: Struct. Chem.* **2015**, *71*, 9–18.
(43) Spek, A. L. Structure Validation in Chemical Crystallography. *Acta Crystallogr., Sect. D: Biol. Crystallogr.* **2009**, *65*, 148–155.
(44) Blatov, V. A.; Shevchenko, A. P.; Proserpio, D. M. Applied Topological Analysis of Crystal Structures with the Program Package ToposPro. *Cryst. Growth Des.* **2014**, *14*, 3576–3586.
(45) Macrae, C. F.; Edgington, P. R.; McCabe, P.; Pidcock, E.; Shields, G. P.; Taylor, R.; Towler, M.; van de Streek, J. Mercury: Visualization and Analysis of Crystal Structures. *J. Appl. Crystallogr.* **2006**, *39*, 453–457.
(46) Burrows, A. D.; Frost, C. G.; Mahon, M. F.; Raithby, P. R.; Renouf, C. L.; Richardson, C.; Stevenson, A. J. Dipyridyl β-Diketonate Complexes: Versatile Polydentate Metalloligands for Metal-Organic Frameworks and Hydrogen-Bonded Networks. *Chem. Commun.* **2010**, *46*, 5067–5069.
(47) Burrows, A. D.; Mahon, M. F.; Renouf, C. L.; Richardson, C.; Warren, A. J.; Warren, J. E. Dipyridyl β-Diketonate Complexes and Their Use as Metalloligands in the Formation of Mixed-Metal Coordination Networks. *Dalton Trans.* **2012**, *41*, 4153–4163.
(48) Guettas, D.; Montigaud, V.; Fernandez-Garcia, G.; Larini, P.; Cador, O.; Le Guennic, B.; Pilet, G. Fine Control of the Metal Environment within Dysprosium-Based Mononuclear Single-Molecule Magnets. *Eur. J. Inorg. Chem.* **2018**, 333–339.
(49) Andrews, P. C.; Deacon, G. B.; Frank, R.; Fraser, B. H.; Junk, P. C.; MacLellan, J. G.; Massi, M.; Moubaraki, B.; Murray, K. S.; Silberstein, M. Formation of Ho^{III} Trinuclear Clusters and Gd^{III}

Monodimensional Polymers Induced by *Ortho* and *Para* Regioisomers of Pyridyl-Functionalised β-Diketones: Synthesis, Structure, and Magnetic Properties. *Eur. J. Inorg. Chem.* **2009**, 744–751.
(50) Liu, F.; Zhou Y. Polymeric $[Eu(L)_3(H_2O)]$ (HL = 1-(Pyridin-4-yl)butane-1,3-dione and Dimeric $[Eu_2(L)_6(H_2O)_2]$ (HL = 1,3-Di(pyridin-3-yl)propane-1,3-dione) as Selective and Sensitive Chemosensors for Hg(II) Ion. *Inorg. Chem. Commun.* **2010**, *13*, 1410–1413.
(51) Brück, S.; Hilder, M.; Junk, P. C.; Kynast, U. H. Synthesis, Structure and Optical Characteristics of Pyridyl Substituted Diketonates of Lanthanoids. *Inorg. Chem. Commun.* **2000**, *3*, 666–670.
(52) Fornies, J.; Navarro, R.; Tomas, M.; Urriolabeitia, E. P. Different Behavior of $(NBu_4)[M(C_6F_5)_2(acac)]$ (M = Pd, Pt) Toward $AgClO_4$. X-Ray Crystal Structures of $(NBu_4)[M_2Ag(C_6F_5)_4(acac)_2]$ (M = Pd, Pt). *Organometallics* **1993**, *12*, 940–943.
(53) Chi, K.-M.; Chen, K.-H.; Peng, S.-M.; Lee, G.-H. Synthesis and Characterization of (β-Diketonato)silver Vinyltriethylsilane Compounds and Their Application to CVD of Silver Thin Films. Crystal Structure of the (2,2-Dimethyl-6,6,7,7,8,8,8-heptafluoro-3,5-octanedionato)silver Vinyltriethylsilane Dimer. *Organometallics* **1996**, *15*, 2575–2578.
(54) Alonso, E.; Fornies, J.; Fortuno, C.; Martin, A.; Orpen, A. G. Reactivity of $[NBu_4][(C_6F_5)_2M(\mu\text{-}PPh_2)_2M'(acac\text{-}O,O')]$ (M, M′ = Pt, Pd) Toward Silver Centers. Synthesis of Polynuclear Complexes Containing M−Ag Bonds (M = Pd, Pt). *Organometallics* **2003**, *22*, 5011–5019.
(55) Khranenko, S.P.; Bykova, E. A.; Gromilov, S. A.; Gallyamov, M. R.; Kozlova, S. G.; Moroz, N. K.; Korenev, S. V. Novel Mixed-Ligand Palladium Complexes $[Pd_2(acac)_3NO_3]$ and $[Pd(acac)NO_3]_n$ Involving O,O- and γ-C-Bonded Acetylacetonate Linkers *Polyhedron* **2012**, *31*, 272–277.
(56) Zhao, Q.; Liu, X. M.; Li, H. R.; Zhang, Y. H.; Bu, X. H. High-performance fluorescence sensing of lanthanum ions (La^{3+}) by a polydentate pyridyl-based quinoxaline derivative *Dalton Trans.* **2016**, *45*, 10836–10841.

Table of Contents Synopsis

Stepwise self-assembly processes using new lanthanide metalloligands and silver salts have been successfully applied to isolate 4f-4d heterometallic coordination networks of four different structural types. Their structures can be rationalized in terms of a new "pincer-like" secondary building unit consisting of a silver cation coordinating the central carbon atoms of two different diketonate ligands.

Table of Contents Graphics